Chapter 6
Surface Preparation Process

6.1 Definition of Process and Target Parameters

6.1.1 Process Parameters

Blast cleaning can be considered to be an erosion process. Erosion is a tribological term, and it can be discussed based on a tribological system. The tribological system for solid particle erosion is schematically shown in Fig. 6.1. The tribological system features the loading collective, the wear parameters and the bodies involved in the process. The loading collective characterises the *process parameters*.

The blast cleaning process is characterised by numerous process parameters that determine efficiency, economy and quality of the whole process. Therefore, optimisation of the process is a primary requirement for a successful application. Generally, the process parameters in blast cleaning divide as listed below (see also Fig. 6.2).

(1) Pneumatic parameters:

- air (nozzle) pressure, p;
- nozzle diameter, d_N;

(2) Process parameters:

- stand-off distance, x;
- impact angle, φ;
- exposure time, t_E;
- number of passes, n_S;

(3) Abrasive parameters

- abrasive mass flow rate, $\dot{m}_P$;
- abrasive particle diameter, d_P;
- abrasive particle size distribution, $f(d_P)$;
- abrasive particle shape;
- abrasive particle hardness, H_P;
- abrasive recycling capacity.

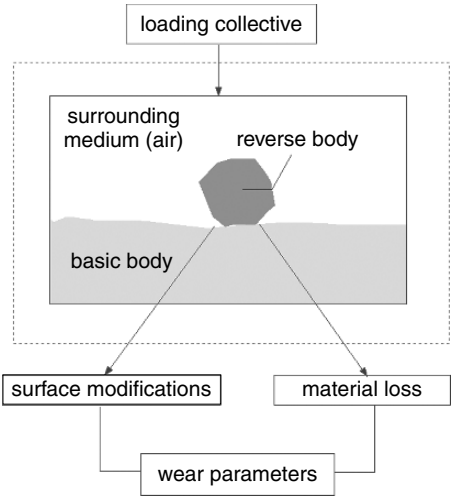

Fig. 6.1 Tribological system for blast cleaning (solid particle erosion)

6.1.2 Target Parameters

The tribological system shown in Fig 6.1 also features wear parameters, which are basically parameters describing material loss and parameters characterising surface modifications. Parameters for the description of surface modifications are discussed in Chap. 7.12.2. Material loss parameters are denoted *target parameters* in this chapter.

Target parameters are illustrated in Fig. 6.2. The most important target parameter in blast cleaning applications is the cleaning rate, which is given as follows:

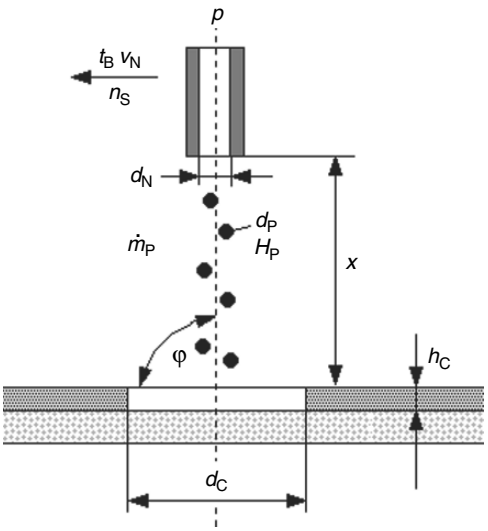

Fig. 6.2 Process parameters and target parameters of blast cleaning processes

$$\dot{A} = \frac{A_M}{t_B} \tag{6.1}$$

In that equation, A_M is the area to be blast cleaned and t_B is the total blast cleaning time. Cleaning rate is usually given in m^2/h. Following an approach of Uferer (1992), the cleaning rate can be expressed in terms of the total kinetic energy of the impinging abrasive particles:

$$\dot{A} = \frac{C_B}{2} \cdot \frac{N_P \cdot m_P}{t_B} \cdot v_P^2 \tag{6.2}$$

The constant C_B is an energy transfer parameter given in s^2/kg. If the thickness of a rust layer or, respectively, a coating system is considered, a volumetric removal rate can be defined as follows:

$$\dot{V}_M = \frac{V_M}{t_B} = \frac{A_M \cdot h_C}{t_B} \tag{6.3}$$

Here, V_M is the removed volume, and h_C is the thickness of the removed material layer. For coatings, h_C equals the dry film thickness. An alternative expression for (6.3) is as follows:

$$\dot{V}_M = A_M \cdot v_N \tag{6.4}$$

Here, v_N is the traverse rate of the nozzle. The unit of the volumetric removal rate is m^3/h.

For optimisation purposes, the consumption of consumable materials need to be considered. The specific abrasive consumption rate, for example, is given as follows:

$$m_S = \frac{\dot{m}_P}{\dot{A}} \tag{6.5}$$

The unit of this parameter is kg/m^2. Similarly, a specific power consumption (kW/m^2) or a specific fuel consumption (l/m^2) could be defined.

6.2 Effects of Pneumatic Parameters

6.2.1 Effects of Air Pressure

Tilghman (1870), in his original patent, wrote: "*The greater the pressure of the jet the bigger will be the velocity imparted to the grains of sand, and the more rapid and powerful the cutting effect upon the solid surface*." In most instances, increasing air pressure increases cleaning rate. A 300% increase in cleaning rate was, for example, reported for the blast cleaning of steel with copper slag if air pressure rose from

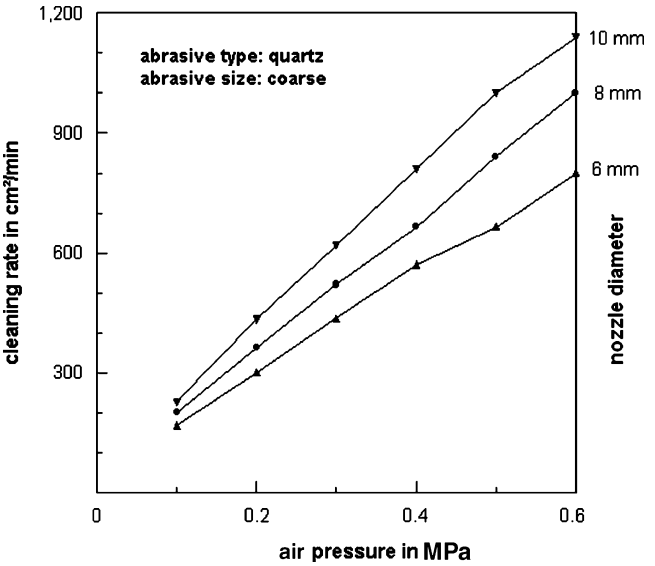

Fig. 6.3 Effects of air pressure and nozzle diameter on cleaning rate (Kalpers, 1949)

$p = 0.53$ to 0.8 MPa (Holt and Austin, 2001). Figures 6.3, 6.4 and 6.9 show general relationships between air pressure and cleaning rate. The higher the nozzle pressure, the more productive is the blast cleaning process in terms of cleaning rate. A linear relationship between air pressure and cleaning rate was also found by Kura (2003) for bar shot, by Kalpers (1949) for grit, and by Seavey (1985) for different non-metallic abrasive materials. A mathematical formulation is:

$$\dot{A} = C_1 \cdot (p - p_C) \tag{6.6}$$

The general structure of this function is the result of complex relationships between pressure and the processes of jet formation, abrasive acceleration and mixing, and material removal. For suction devices, cleaning rate rises according to a square-root relationship with increasing air pressure (Uhlmann et al., 2003). Figure 6.4 provides further insight into the effect of air pressure on cleaning rate. It can be recognised that the pressure influence depended on abrasive material. In the case of copper slag, cleaning rate even dropped at high pressure levels, an effect which can be explained through the friability of this material. At high pressures, this material is fractured in the nozzle and on the substrate surface. Such trends were reported by Gesell (1966) for quartz, copper slag and foundry slag. More information on this issue is delivered in Sect. 2.9. Although (6.6) holds for many cases, the real process can differ from a linear relationship, especially if rather hard target materials are being treated.

The first stage, $p < p_C$, characterises an *incubation stage*. In this pressure range, no material removal takes place, although the removal process is invisibly introduced in the material. The parameter p_C is a threshold value that has to be

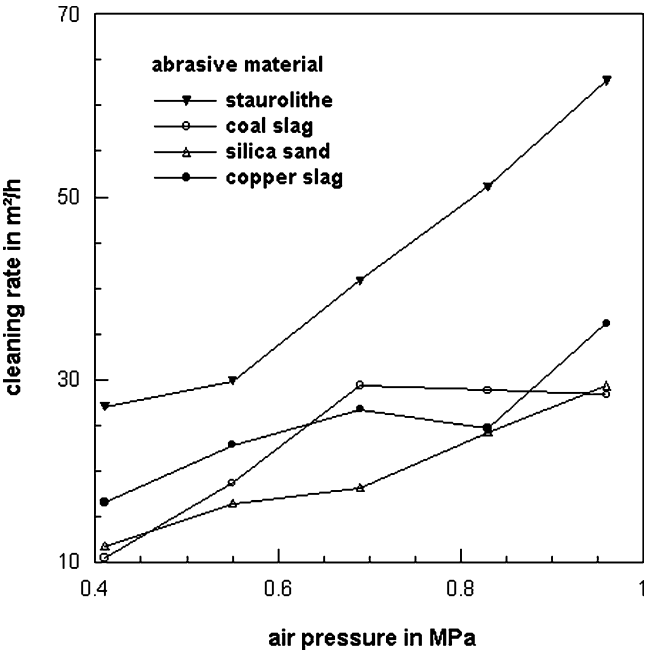

Fig. 6.4 Effects of air pressure and abrasive material on cleaning rate (Seavey, 1985)

exceeded for a measurable material removal. Results of Uferer (1992) deliver a value of $p_C = 0.05$ MPa for the removal of mill scale from steel plates with nickel slag. The threshold pressure could be interpreted as a critical particle impact velocity, which is known from impact testing of organic coatings (Breinsberger and Koppelmann, 1982; Ladstädter, 1984). For elastically responding materials, say mill scale, heavy rust or brittle coatings, a threshold concept developed by Evans et al. (1978) for solid particle erosion can be applied. In this model, the threshold velocity of the particles is given by the following equation:

$$v_C \propto K_{Ic}^2 \cdot c_M^{0.33} \tag{6.7a}$$

In that equation, K_{Ic} is the fracture toughness of the target material, and c_M is the velocity of longitudinal waves in the target material. Values for the fracture toughness of some organic coating materials are listed in Table 5.11. This approach is partly verified by the experimental results presented in Fig. 6.5. For plastically responding materials, say soft coatings and most metal substrates, a rather complex model introduced by Yabuki and Matsumura (1999) can be applied. One basic result of this model is that the threshold velocity, required for micro-cutting, has a linear relationship with the material hardness:

$$v_C \propto H_M \tag{6.7b}$$

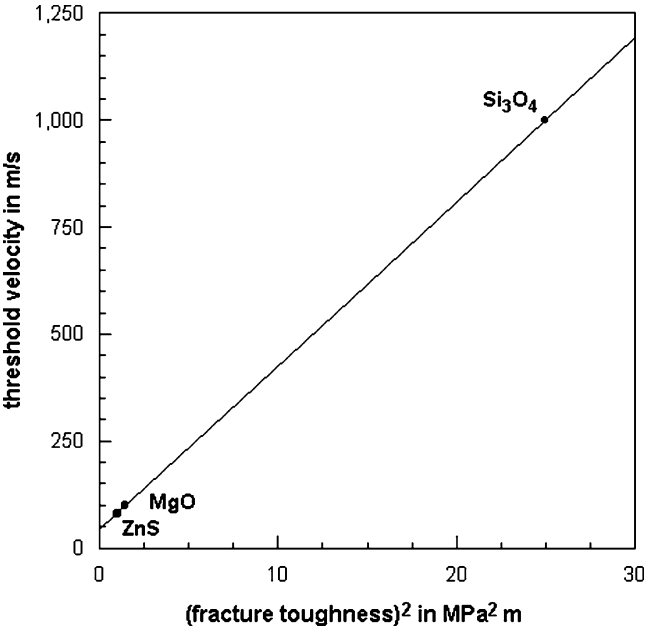

Fig. 6.5 Relationship between threshold particle impact velocity and fracture toughness for brittle target materials (Evans et al., 1978)

Hardness values for some coating materials are listed in Tables 5.1, 5.3 and 5.7–5.10. The threshold values, measured on numerous metals, were too low (between $v_C = 1$ and 3 m/s) that they do not need to be considered in practice (Yabuki et al., 1999). Luo et al. (2001) estimated threshold velocities between $v_C = 6$ and 7 m/s for the slurry erosion of fusion-bonded epoxy powder coatings. Another threshold characteristic is illustrated in Fig. 5.21b, which illustrates the situation for material detachment in a plastically deformable material. It can be seen that a critical particle impact velocity must be exceeded before material removal starts. This value is at about $v_P = 210$ m/s for the situation illustrated in Fig. 5.21b. If this velocity value is not reached, the material only deforms.

Papini and Spelt (1997) provided the idea that coating removal begins only when the coating is fully penetrated for a given coating/substrate/particle system. They derived a critical abrasive impact velocity to cause penetration of the coating to the steel substrate, and they provided a methodology for the calculation of these velocity values. The normal component of the critical penetration velocity increased with larger coating thickness, which was attributed to a relationship between coating thickness and interface shear stress. Typical values for the penetration of alkyd paint layers (DFT = 20–50 µm) were between $v_C = 20$ and 45 m/s. Later, these authors (Papini and Spelt, 1998b) introduced a critical particle energy required for the introduction of coating delamination. This relationship is illustrated in Fig. 5.60, and it can be seen that the threshold energy depended on the coating thickness.

In the second stage, $p > p_C$ – called *linear stage* – cleaning rate increases linearly with an increase in air pressure. Each increase in air pressure leads to a proportional increase in cleaning rate. The factor of proportionality C_1 depends on all the process conditions listed earlier as well as on the properties of the target material. Figure 6.3a reveals a slight effect of the nozzle diameter. For the linear coefficient C_1 exists the following rule of thumb: "*For each 7 kPa increase* (*in pressure*) *there is a 1.5 percent increase in productivity.*" (Drisko, 2002). However, results published by Seavey (1985) have shown that C_1 depended on the abrasive material used. Some results of this investigation are plotted in Fig. 6.4. It can be seen that the proportionality factor was rather low for quartz and coal slag, and that it was higher for copper slag and fine-grained staurolite. In some cases, cleaning rate can even drop if pressure is increased. Such phenomena were reported by Seavey (1985) for the use of coal slag. This feature is illustrated in Fig. 6.4. The reason for this behaviour could be the high degree of friability of the slag material. If the pressure, and thus the abrasive particle impact velocity, becomes too high, the slag particles start to fracture during the impact process and do not work efficiently (see Fig. 6.4). Similar is the situation if rather large abrasive particles are being used, as has been observed by Stallmann et al. (1988) for copper slag and melting chamber slag. It is, therefore, a general recommendation to select an air pressure lower than, or close to, the critical pressure for abrasive impact fragmentation. More information on this issue is provided in Sect. 2.9. Results plotted in Fig. 6.9 show that the coefficient C_1 depends also on the nozzle geometry.

Air pressure determines the velocity of the impinging abrasive particles (see Sect. 3.6.1). This fact was considered by Settles and Garg (1995) who calculated the abrasive particle velocities for the cleaning rate examples provided in Fig. 6.4. They computed the following values for the particle velocity ($p = 0.7$ MPa, $d_N = 9.5$ mm; $\dot{m}_P = 9.7$ kg/min): $v_P = 173$ m/s for the silica sand and $v_P = 210$ m/s for the staurolite. From these results, they concluded that the high productivity of the staurolite abrasive is a result of the higher abrasive particle impact velocity.

Abrasive particle velocity has the strongest influence on the erosion durability of organic coatings, if abrasive size, temperature, impact angle and abrasive particle velocity are being considered (Trezona et al., 2000a). For polymeric paint films, a power-law dependency of the erosion resistance (given in kg/m^2) on the abrasive particle velocity can be expected (Rutherford et al., 1997). The following relationship can be assumed:

$$R_E \propto \frac{1}{v_P^q} \tag{6.8}$$

Here, q is a velocity exponent. By fitting experimental results obtained with multi-layer organic coating systems applied to galvanised steel substrates, this exponent was found to be $q = 3.5$ (Rutherford et al., 1997), which points to a stronger relationship as for the erosion of bulk polymers ($q = 2.5$).

Particle impact velocity affects the erosion rate according to a power law. A suitable relationship is as follows:

$$E_R \propto v_P^{\phi} \tag{6.9}$$

A simple model developed by Rosenberger (1939) for blast cleaning processes delivered a velocity parameter of $\phi = 2.0$.

Power exponents for brittle material removal modes are listed in Table 5.13. Power exponents for polymer coatings (for hydroabrasive erosion) are listed in Table 6.1. For rubber, the power exponent depended on the fatigue-function parameter β_F (see Sect. 5.6.4). Detailed relationships were $\phi = 2 \cdot \beta$ for normal impact angles; and $\phi = \beta_F + 1$ for oblique impact angles (Arnold and Hutchings, 1992, 1993). Slikkerveer (1999) found values between $\phi = 2.87$ and 4.0 for different elastomers, whereby the high value characterised the behaviour of the most "rubber-like" material. For polymers, power exponent values between $\phi = 1.7$ and 2.8 were found (Zhang et al., 1995); and for the slurry erosion of fusion-bonded epoxy powder coatings, power exponents between $\phi = 4.0$ and 5.5 were reported (Luo et al., 2001). A power law with $\phi > 1$ could also describe the influence of the particle velocity on the volume of removed lips during the erosion of polymers (Walley and Field, 1987). Henning and Brauer (1986) found that the power exponent depended on impact angle and abrasive diameter. For PMMA, the exponent was found to vary between $\phi = 2.7$ and 3.2, whereas the latter value was for high impact angles. For rubber, values between $\phi = 2.5$ and 5.0 were found, whereby the precise value depended on the diameter of the impinging particles. Volume loss measurements performed by Tangirala (1998) on brittle iron scale delivered a power exponent slightly larger than unity.

If the Almen intensity was being considered as the target parameter, which is a familiar procedure in shot peening applications, the relationship between shot velocity and Almen intensity was linear (Linnemann et al., 1996).

Rajesh et al. (2004) investigated the effects of impact angle and material type on the particle impact velocity effects. They eroded seven types of polyamides at impact velocities of $v_P = 80$ m/s and, respectively, $v_P = 140$ m/s, which was a velocity increase of +75%. Their results are listed in Table 6.2, and the results witnessed a notable effect of the impact angle on the percentage of increase in the erosion rates. The highest increase of +240% was found for PA11 impinged at an angle of $\varphi = 30^\circ$. For an impact angle of $\varphi = 90^\circ$, however, the increase in erosion rate due to the higher impact velocity was +79% only. For the material PA12, the gain in erosion rate was larger for the high impact angle, which was not found for the other materials.

Fokke (1999) investigated the relationships between the kinetic energy of impinging abrasive particles, the impact area and the volume removed in epoxy-based

Table 6.1 Velocity exponents for polymer coatings (Zolotar, 1973); hydroabrasive erosion, $v_P = 5$–17 m/s

Material	Velocity exponent
Epoxy	3.06
Epoxy-phenol formaldehyde resin	3.20
Methacrylate resin	3.13
Phenol formaldehyde liquid	3.10
Vulcanite	3.02
Phenol formaldehyde powder	3.40

Table 6.2 Percentage increase in erosion rate for an impact velocity increase from $v_P = 80$ m/s to $v_p = 140$ m/s (Rajesh et al., 2004). Variable impact angle

Polyamide	Increase in erosion rate in %	
	30°	90°
PA 6	180	70
PA 11	240	70
PA 12	190	60
PA 12 (L 20)	160	210
PA 66	180	130
PA 66/610	220	30
Aromatic PA	200	50

organic coatings. For the blast cleaned area as the target parameter, the following linear trend was found:

$$A_M = \varepsilon_M \cdot E_P \tag{6.10}$$

The coefficient ε_M is the inverse specific erosion energy (m^2/J), and it depends on impact angle. The inverse specific energy decreased notably if impact angle increased (Fokke, 1999). The volume of removed paint showed a power-law relationship to the impact energy:

$$V_M = 3.1 \cdot 10^{-13} \cdot E_P^{1.5} \tag{6.11}$$

Here, V_M is given in m^3, and the particle impact energy is given in mJ. Results of measurements are presented in Fig. 6.6. The power exponent of 1.5 is right between two exponents estimated by Wood (1999) for the erosion of different metallic and ceramic coatings by a slurry flow. This author found a value of 1.17 for normal impact angles, and a value of 1.98 for an oblique ($\varphi = 30°$) impact angle.

Some results from scale removal experiments (with blast wheels) are provided in Fig. 6.7. The graph shows critical energy conditions for scale removal as functions of impact velocity, abrasive diameter and particle kinetic energy. This graph very well supports the threshold conception mentioned earlier. The removal of the mill scale becomes possible only if a certain impact velocity is exceeded for a given abrasive size. The effect of the impact velocity was pronounced in the range of small abrasive particles. Although these results were obtained with a wheel blast machine, the basic idea will work the same way for air blast machines.

6.2.2 Effects of Nozzle Diameter and Nozzle Length

Figure 6.8 shows typical relationships between cleaning rate and nozzle diameter for two air pressure levels. The cleaning rate almost linearly increases with an increase in the nozzle diameter. A simple expression is:

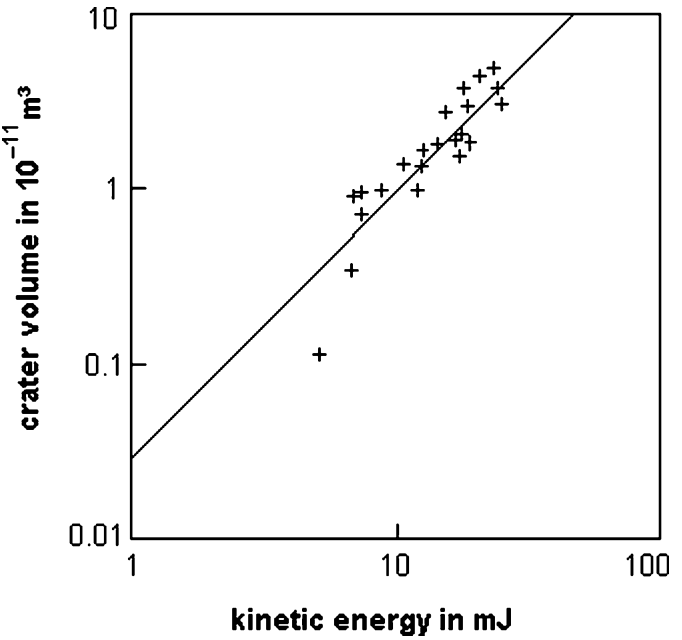

Fig. 6.6 Effect of particle kinetic energy on volume of removed paint (Fokke, 1999)

$$\dot{A} = C_2 \cdot d_N^{\chi_N} \tag{6.12}$$

with $\chi_N < 1$.

The major contribution of the nozzle diameter to the material removal process is the determination of air mass flow rate as well as of abrasive mass flow rate (if a fixed ratio between air mass flow rate and abrasive mass flow rate is desired). Both parameters increase if nozzle diameter rises (see Sects. 3.2 and 4.3.2). Nozzle diameter also affects the size of the blasted area (see Sect. 3.4). A threshold diameter does not seem to exist, although practice shows that a minimum nozzle diameter should not be undercut in order to realise a satisfying performance. The proportionality factor C_2 seems to decrease slightly with an increase in air pressure for the conditions in Fig. 6.8.

It is important to note that a trend as shown in Fig. 6.8 can be realised only if the compressor can deliver a volumetric air flow rate high enough to meet the requirement of a larger nozzle diameter. If the compressor cannot be adjusted to an increasing nozzle diameter, the working lines of compressor and nozzle will not intersect (see Fig. 4.3). The cleaning rate will drop if the nozzle diameter increases. This case is illustrated in Fig. 4.37, where the drop in cleaning rate for the larger nozzle diameter is almost 40%. The reason is the pressure drop in the system which leads to a deteriorated cleaning process. The limit for an increase in nozzle diameter is, therefore, the capacity of the compressor.

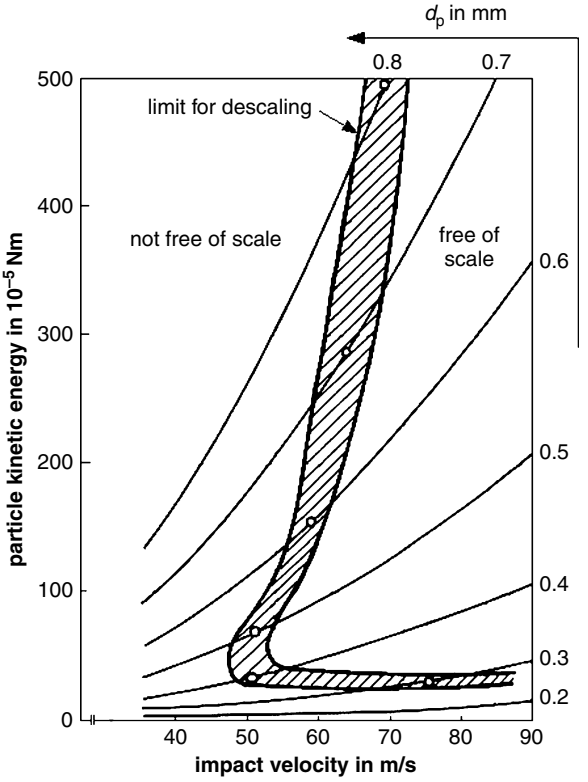

Fig. 6.7 Threshold conditions for mill scale removal from steel substrates (Weidenhaupt, 1970)

Uferer (1992) introduced a nozzle-shape factor, f_N, which depends on nozzle length. Cleaning rate is assumed to rise linearly with an increase in this parameter. For cylindrical nozzles, f_N depends on nozzle length; and for Laval nozzles, f_N depends on air pressure. Table 6.3 lists some typical values. According to these values, Laval nozzles would provide a higher cleaning rate.

6.2.3 Effects of Nozzle Design

A number of investigations depicted a notable influence of nozzle design parameters on the efficiency of blast cleaning processes. Djurovic et al. (1999), for example, noted an effect of the nozzle cross-section shape on the removal of organic coatings from aluminium substrates with starch media. The width of the traces formed in the paint layer was 26 mm for a round nozzle exit, but 46 mm for a rectangular nozzle exit; this was an increase of about 180%. It is also known that the energy distribution at the target surface notably depends on the nozzle exit geometry. These relationships are displayed in Figs. 3.33, 3.34 and 3.51.

Further effects of nozzle geometry were investigated by Kline et al. (1988) and Plaster (1972). Results of descaling tests with different nozzle types are summarised

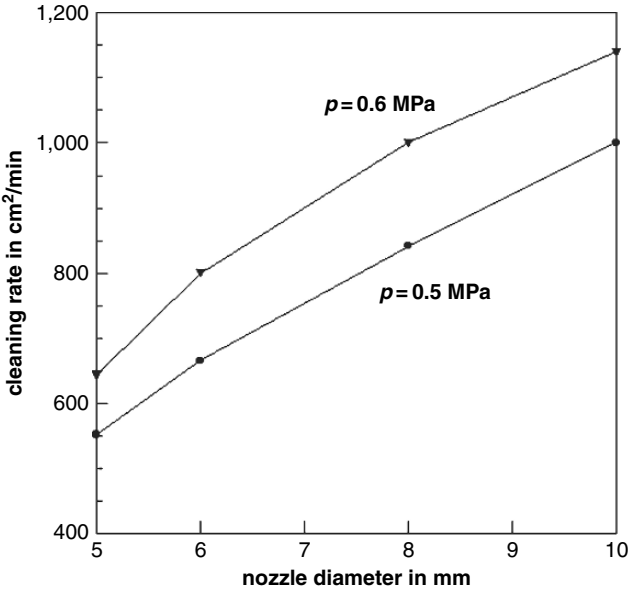

Fig. 6.8 Effect of nozzle diameter on cleaning rate (Kalpers, 1949)

in Fig. 6.9. It can be seen that scale mass loss rate increased with increasing pressure for all nozzle types, which verifies the trends discussed in Sect. 6.2.1. However, the individual trends depended on nozzle geometry. The maximum mass loss was obtained at all pressure levels if a convergent–divergent (Laval) nozzle was utilised. For the highest pressure level, however, this advantage vanished, and a divergent nozzle with a bell-shaped inlet section performed equally.

Kline et al. (1988) performed laboratory and site experiments with a number of different nozzles at higher compressor pressures. The authors cleaned mill scale bearing steel plates to a near-white surface standard, and they tested four different types of nozzles: a standard Laval nozzle, a nozzle with wide throat design, a double Laval

Table 6.3 Blasting nozzle coefficient f_N (Uferer, 1992)

Cylindrical nozzle	
Nozzle length in mm	f_N
50	0.60
80	0.85
100	0.93
120	1.00
150	1.05
Laval nozzle	
Nozzle air pressure in MPa	f_N
<0.3	1.0–1.1
0.3–0.6	1.1–1.3

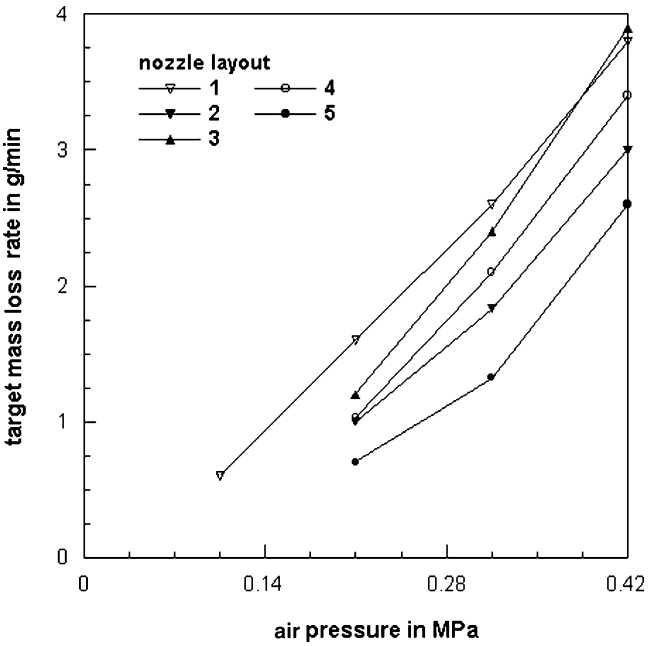

Fig. 6.9 Effects of nozzle design and nozzle pressure on the removal of mill scale (Plaster, 1972). Nozzle layout: 1 – convergent–divergent (Laval) nozzle; 2 – bell-mouthed convergent nozzle; 3 – bell-mouthed divergent nozzle; 4 – bell-mouthed convergent–divergent (Laval) nozzle; 5 – convergent-parallel nozzle (lined with tungsten carbide sections). Abrasive type: crushed chilled cast iron shot; nozzle diameter: $d_N = 9.5$ mm

nozzle and a Laval nozzle with a distinctively large exit end opening. Results of these investigations are plotted in Figs. 6.10 and 6.11. The graph in Fig. 6.10 provides results of laboratory tests. No apparent improvement could be achieved with the wide throat nozzle. This design will benefit only from a larger blast hose that is able to take advantage of the wider throat cross-section (see Sect. 4.5). The double Laval nozzle gave little or no significant improvement compared to the standard Laval design. Productivity could significantly be improved by using the wide exit opening design; the results indicated an improvement of about +50%. The gain was probably due to the larger blast pattern obtained with this nozzle. Measurements of the blast pattern sizes indicated a diameter of 102 mm for the wide exit opening nozzle compared to a diameter of 76 mm for the standard Laval nozzle. Results of field tests are plotted in Fig. 6.11. A laminar flow nozzle was included to these tests, which featured a very smooth transition throat between the convergent and divergent nozzle sections. This design did not deliver a productivity improvement. The double Laval nozzle generated about +10% more productivity improvement over the standard Laval nozzle at all pressure levels. The large exit opening design was significantly more effective than the standard Laval nozzle at the two higher pressure levels. A higher nozzle pressure was beneficial to the cleaning efficiency for all nozzle types, but it was most influencing if the large exit opening design was utilised.

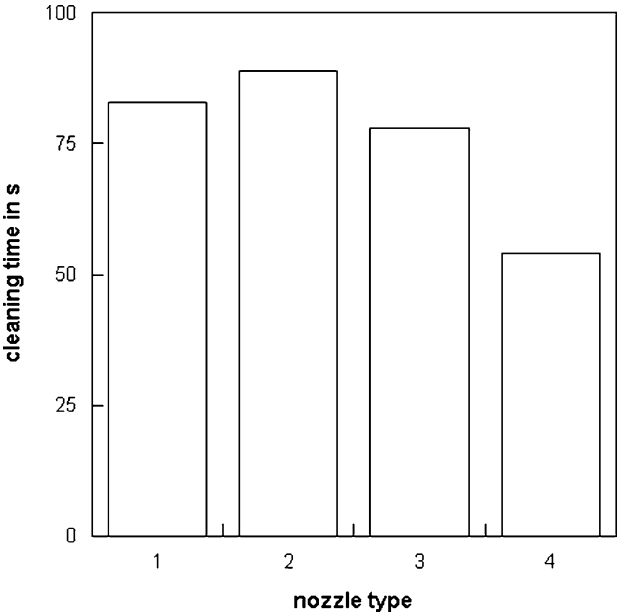

Fig. 6.10 Effects of nozzle design and nozzle pressure on the removal of mill scale (Kline et al., 1988); results of laboratory tests. Nozzle layout: 1 – standard Laval nozzle; 2 – nozzle with wide throat; 3 – double Laval nozzle; 4 – nozzle with distinctively large exit opening

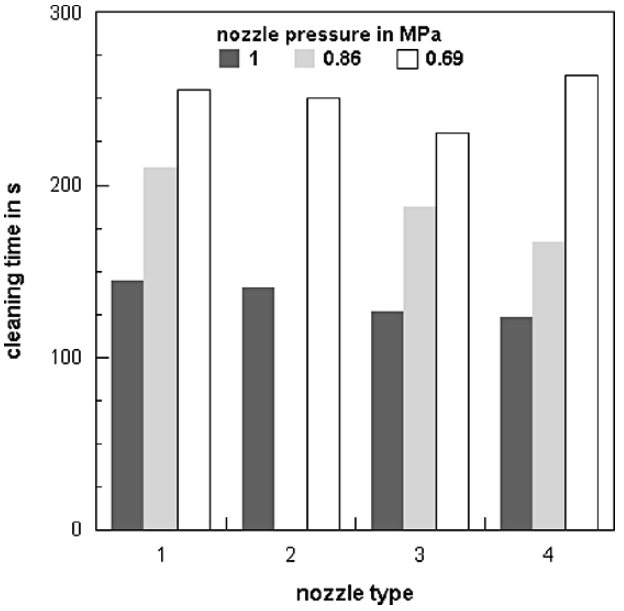

Fig. 6.11 Effects of nozzle design and nozzle pressure on the removal of mill scale (Kline et al., 1988); results of site tests. Nozzle layout: 1 – standard Laval nozzle; 2 – laminar flow nozzle with soft flow transition; 3 – double Laval nozzle; 4 – nozzle with distinctively large exit opening

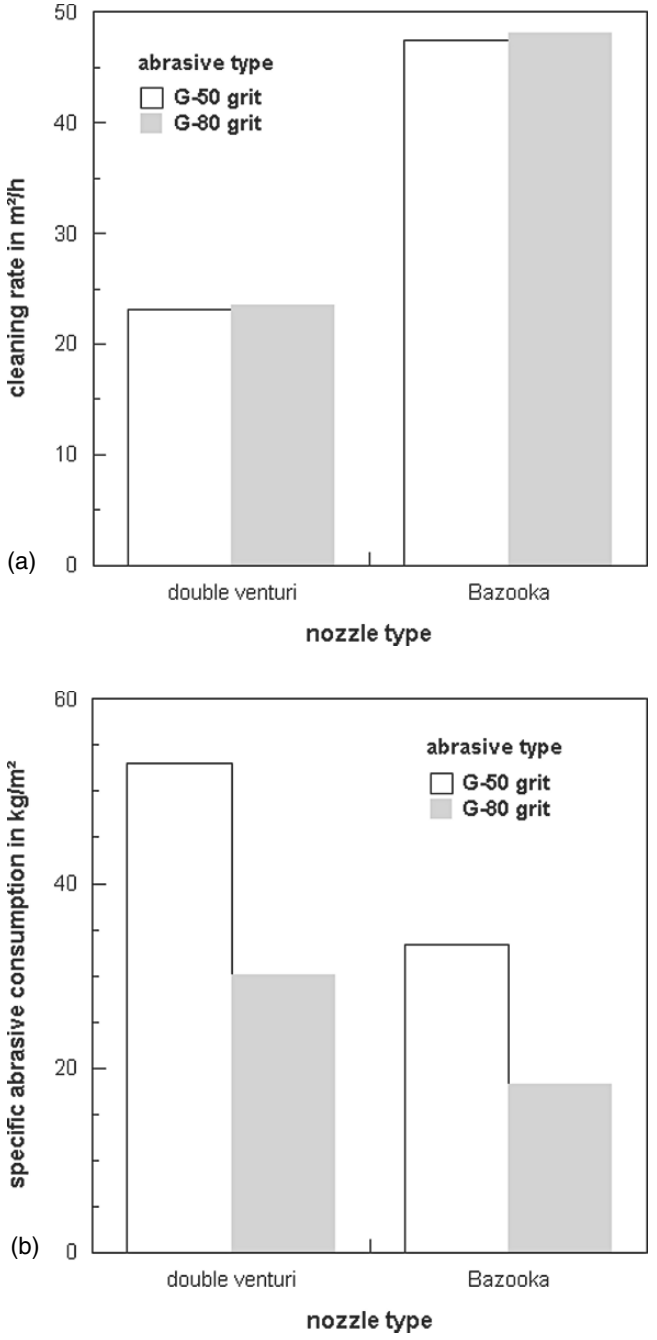

Fig. 6.12 Effects of nozzle design and abrasive type on target parameters (Hitzrot, 1997). "Double venturi" corresponds to nozzle "3" in Figs. 6.10 and 6.11; "Bazooka" corresponds to nozzle "4" in Figs. 6.10 and 6.11. (**a**) Effects on cleaning rate; (**b**) Effects on abrasive consumption

Figure 6.12 illustrates the effects of abrasive particle size on the nozzle design. With respect to cleaning rate, shown in Fig. 6.12a, the size of the abrasives did not affect the cleaning rate for a given nozzle design. The Bazooka nozzle type delivered higher efficiency values compared with the double Laval nozzle, whether small or large steel grit particles were used. If, however, the specific abrasive consumption was considered, the situation changed. This aspect is illustrated in Fig. 6.12b. The double Laval nozzle, fed with smaller steel grit particles, was more efficient than the Bazooka type nozzle, fed with larger steel grit particles. For a given nozzle design, abrasive size affected the specific abrasive consumption notably, whereby the smaller steel grit particles led always to a more efficient performance.

Figure 6.13 displays results of erosion experiments performed by Hamann (1987) with different nozzle configurations. Figure 6.13a applies to the removal of mill scale from steel plates with steel shot, whereas Fig. 6.13b applies to the removal of a PVC plate with nickel slag. It can be recognised that a convergent–divergent nozzle with a specially designed inlet section (nozzle type "4") was the most effective design for both experimental situations. With regard to the removal of the mill scale, a cylindrical nozzle with a bell-shaped inlet section (nozzle type "2") was more efficient than a convergent–divergent nozzle (nozzle type "3"). However, the opposite trend could be found during the treatment of the PVC targets, where the convergent–divergent nozzle performed more effective. It can also be seen that a convergent–divergent nozzle with a short convergent section (nozzle type "2") was very efficient for the removal of mill scale, but it did not show an equally good performance during the treatment of the PVC samples.

A convincing conclusion from the presented results is that an optimum nozzle design does not exist in general. The nozzle design must be adapted to the entire cleaning system, which include abrasive material, process parameters and target material response.

Hutans (1986) placed a pipe between nozzle exit and surface to be blast cleaned in order to reduce the effects of interactions between the abrasive-air flow and the surrounding air. He reported notable improvements in terms of cleaning rate, specific abrasive consumption and specific energy consumption. The savings were larger for blast cleaning in an open environment compared to blast cleaning in a hall.

6.3 Effects of Performance Parameters

6.3.1 Effects of Stand-off Distance

Results of Remmelts (1969) on the effect of variations in stand-off distance on the cleaning rate for mill scale are displayed in Fig. 6.14. Such a trend was also found for the removal of coatings from metal substrates (Uhlmann et al., 2003). Three regions can be distinguished in the graph: an initial region, an optimum region and a decreasing region. The optimum stand-off distance is in the range between $x = 57$ and 67 mm. These values are close to the SSPC Surface Preparation Commentary,

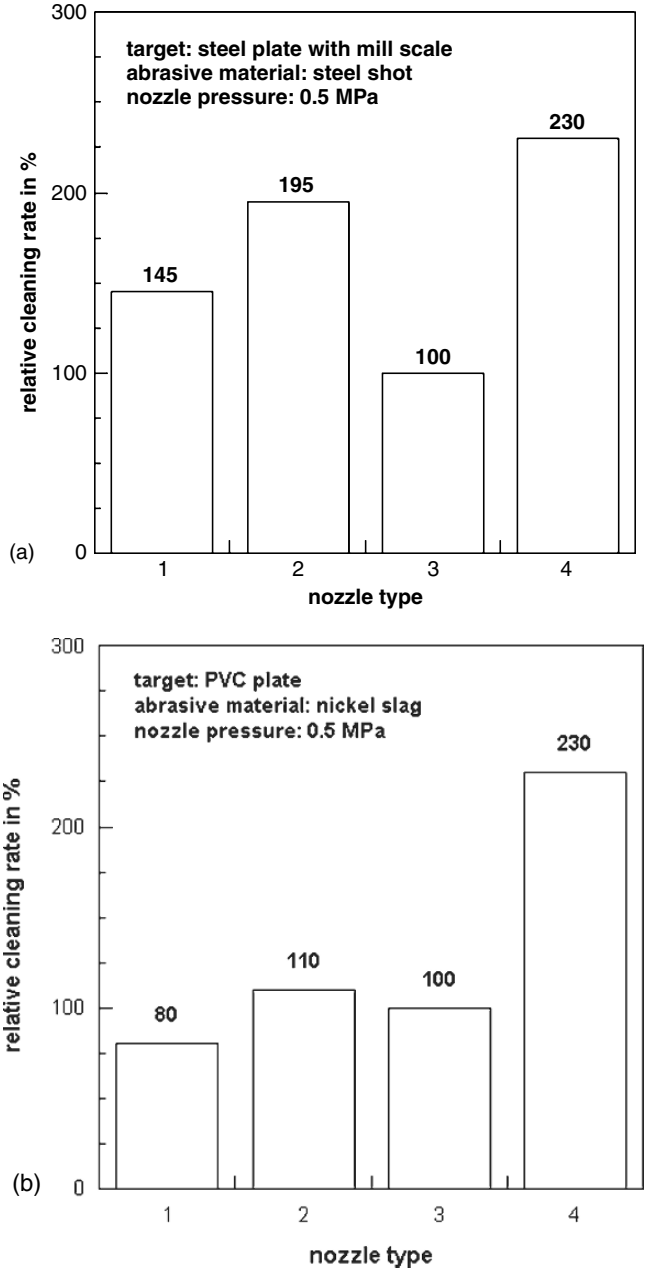

Fig. 6.13 Effects of nozzle design on material removal efficiency (Hamann, 1987). Nozzle layout: 1 – cylindrical nozzle with bell-shaped inlet section; 2 – divergent–convergent nozzle with short divergent section; 3 – standard divergent–convergent nozzle (Laval); 4 – divergent–convergent nozzle with additional inlet flow section. (**a**) Removal of mill scale from steel plates with steel grit; (**b**) Erosion of PVC samples with nickel slag

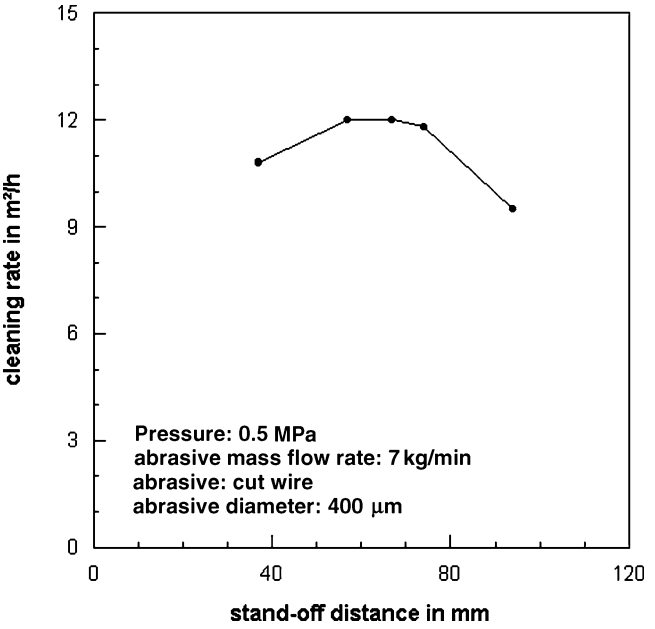

Fig. 6.14 Effect of stand-off distance on cleaning rate for mill scale (Remmelts, 1969)

which states the following: *"For optimum cleaning rate, the nozzle to surface distance is around 46 cm."* This optimum distance can vary depending on the type of substrate, material to be removed and process parameters to be adjusted. An older regulation for the removal of mill scale and rust from ship steels due to blast cleaning recommended optimum stand-off distances between $x = 40$ and 60 cm (STG, 1963).

It was shown in Sect. 3.6.6 that abrasive particle velocity increases further after the particles have exited the nozzle (see Figs. 3.46 and 3.47). This phenomenon explains partly the existence of an optimum stand-off distance for blast cleaning processes. Another aspect is the increase in jet diameter and, thus in the size of the blasted area (see Fig. 3.22). This issue is discussed in Sect. 3.4.

Uferer (1992) introduced a stand-off distance parameter f_X, whose values are listed in Table 6.4 for different abrasive materials. It can be seen that slag and quartzsand are much more sensitive to variations in stand-off distance than steel

Table 6.4 Values for the stand-off distance coefficient f_X for the removal of rust (Uferer, 1992)

Abrasive material	Value for f_X				
	Stand-off distance in mm				
	250	300–400	500	600	750
Steel wire	–	0.90	1.00	1.00	1.00
Slag and quartz	0.95	1.05	1.00	0.85	0.65

wire. This result agrees with the trends shown in Fig. 3.40, where it can be seen that the increase in particle velocity after the nozzle exit was more distinct for the slag material (at least for the convergent–divergent nozzle).

6.3.2 Effects of Relative Particle Distance

The relative distance between particles in the particle stream according to (3.45) affects the erosion of materials. Results cited by Ciampini et al. (2003a) showed a drop in erosion rate from a constant value of unity for low L_P*-values to much lower erosion rates at a L_P* of about 17. This result was attributed to a sudden increase in interference between incidental and rebounding particles at the higher L_P*-numbers.

Balasubramaniyan (1998) has shown that the volume loss of eroded brittle materials was very sensitive to changes in the relative particle distance if $L_P^* < 1$. This would mean that changes in the stream density are critical to the material removal process for $\rho_S^* > \pi/6$.

6.3.3 Effects of Impact Angle

The effect of variations in impact angle on the cleaning rate for mill scale is displayed in Fig. 6.15 for two abrasive mass flow rates. A maximum cleaning rate could be noted at an angle of $\varphi = 45^\circ$ which is rather typical for plastically responding materials. The lowest cleaning rate was found at perpendicular impact for both parameter conditions. These results neither verified the general recommendation in the SSPC Surface Preparation Commentary: "*An 80 to 90 degree angle is best suited for removing mill scale or heavy rust and for cleaning pitted areas*", nor did the scale removal model presented in Sect. 5.6. However, abrasive mass flow rate seemed to play an additional role, as illustrated in Fig. 6.15, and the lower value for the abrasive mass flow rate did not reveal a "ductile" behaviour of the scale. If elastically responding materials, namely heavy rust, heavy mill scale, brittle coatings, need to be removed, a normal impact angle is often the right choice. Averchenko et al. (1970), for example, determined maximum values for the erosion rate of brittle enamel coatings at normal impact angles. For the removal of rust (no platy rust) from steel plates, Uferer (1992) found an increase in cleaning rate if impact angle rose from $\varphi = 45^\circ$ to 90°. Tangirala (1998) noted a maximum volume loss of iron scale if the impact angle was $\varphi = 90^\circ$.

Maximum erosion rates at low impact angles are rather typical for materials being removed by micro-cutting or, respectively, ploughing processes (see Sect. 5.5.2). Such trends were also observed for organic coating materials by Kotnarowska (2003), Zahavi and Schmitt (1981, 1982) and Trezona et al. (2000a); for rubber by Arnold and Hutchings (1992) and Slikkerveer (1999); for enamel coatings by Parslow et al. (1997) and for polyethylene by Walley and Field (1987).

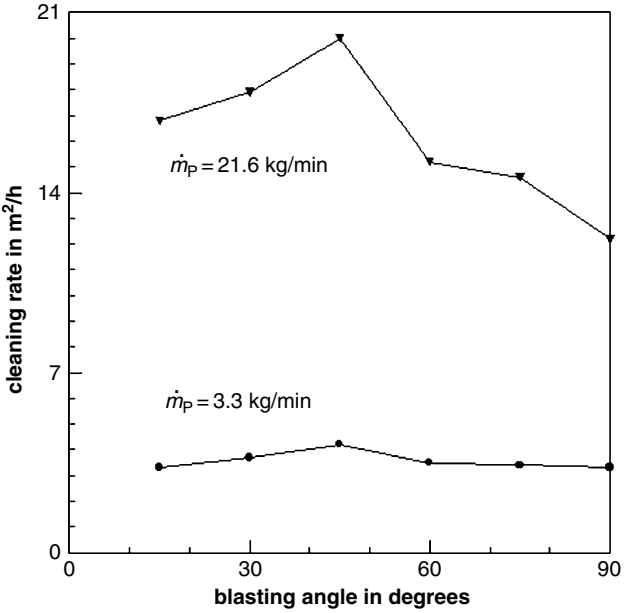

Fig. 6.15 Effects of blasting angle and abrasive mass flow rate on cleaning rate for mill scale (Remmelts, 1969)

An example is provided in Fig. 6.16 which shows that the type of the epoxy coating system did not affect the location of the optimum impact angle. Zahavi and Schmitt (1981, 1982) eroded rather thin organic coatings (DFT between 30 and 75 µm) with quartz sand (d_P = 210–297 µm) at a moderate impact speeds (v_P = 42 m/s) and investigated the effects of impact angle variations. They found that changes in impact angle were more affective to the erosion of rather hard polyurethane coatings. For elastomeric coating materials, the mass loss due to erosion was almost unaffected if the impact angle exceeded a value of about $\varphi = 45^\circ$.

Optimum impact angles for the erosion of rubber by impinging solid particles were found between $\varphi = 15^\circ$ and 20° (Arnold and Hutchings, 1992). Slikkerveer (1999) derived the following relationship between impact angle and erosion rate of rubber materials:

$$E_R = a \cdot (1 + b \cdot \cos^c \varphi) \tag{6.13}$$

The regression parameters had the following values: a = 0.0072–0.037; b = 2.7–8.7 and c = 2.2–8.0. The regression parameter a is the erosion rate at normal impact ($\varphi = 90^\circ$), and the parameter c describes the transition from oblique to normal impact.

Fokke (1999) introduced the inverse specific erosion energy [see (6.10)], and he found a dependence with the impact angle. The inverse specific erosion energy decreased with an increase in impact angle in the impact angle range between $\varphi = 30^\circ$

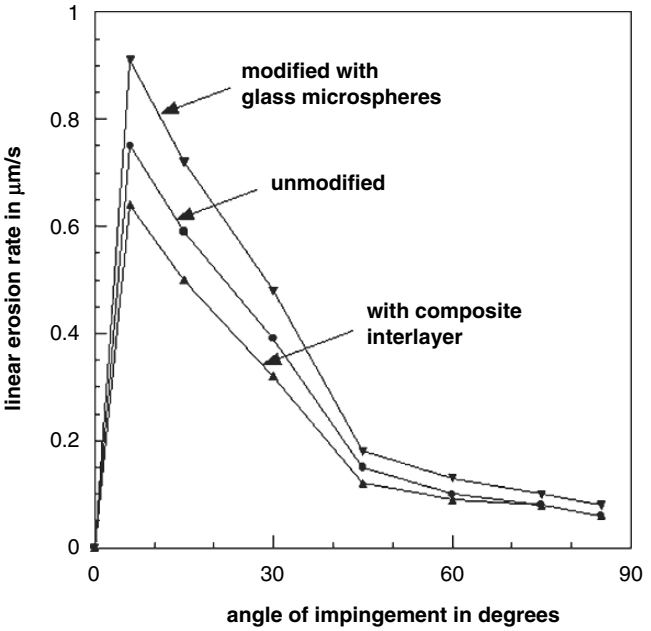

Fig. 6.16 Effect of blasting angle and coating composition on coating removal (Kotnarowska, 2003)

and 45°. For impact angles larger than $\varphi = 45°$, impact angle did not affect the inverse specific erosion energy.

Uferer (1992) introduced an impact angle factor f_ϕ, which has a linear effect on the cleaning rate for the removal of mill scale and rust. Typical values for this parameter are listed in Table 6.5.

6.3.4 Effects of Exposure Time

Removal rate and cleaning rate increase with an increase in exposure time. The respective functional relationship can be described as follows:

$$\dot{A} \propto (t_E - t_I)^{n_t} \tag{6.14}$$

Table 6.5 Values for the blasting angle coefficient f_ϕ (Uferer, 1992)

Blasting angle	Coefficient f_ϕ	
	For mill scale	For rust
30°	1.5	–
45°	1.6	0.6
60°	1.25	–
90°	1.0	0.84

This relationship can be considered a removal kinetics, whereby values for the exponent range between $n_t = 0$ and 1. Therefore, the efficiency of cleaning processes and of material removal processes drops with an increase in exposure time. If the deposit or coating is completely removed from a substrate, $n_t = 0$. It was shown that the precise values for n_t depended, among others, on abrasive type and size (Raykowski et al., 2001). Some relationships are listed in Table 6.6. The parameter t_I is an incubation period which must be exceeded in order to generate a measurable material removal. Equation (6.14) has the same structure as (5.47), which was derived by Schmithals (1961) for the blast cleaning of mill scale.

An alternative exposure parameter is the local exposure time, which is given as follows:

$$t_E = d_J / v_N \tag{6.14a}$$

The jet diameter can sometimes be replaced by the nozzle diameter ($d_J = d_N$). A general plot of local exposure time versus volumetric erosion is shown in Fig. 6.17. It can be seen that the erosion rate (slope of the curve) increased notably at low exposure times. If the local exposure time increases further, efficiency (in terms of the slope of the curve) dropped. From this point of view, short local exposure times (high traverse rates) are recommended. A threshold exposure time (t_I), which separates the incubation period from the erosion period, is also shown in Fig. 6.17. A threshold (incubation) period was found by Friedrich (1986) for the particle erosion of polymers. The actual magnitude of the incubation time depended on the brittleness of the polymers. More brittle polymers did not exhibit a notable incubation period. D'Emanuele et al. (1992) found for copolymer materials that the duration of the incubation period depended on the initial molecular weight of the polymers. These authors characterised the incubation period as a time during which a rapid decrease in polymer molecular weight occurred. Threshold periods are also known from other abrasive jet applications, namely hydroabrasive machining (Momber and Kovacevic, 1998), but also from hydroblasting applications (Momber, 2003, 2005a). The most probable explanation is that erosion of the coating starts after a period of damage accumulation by subsequently impinging abrasive particles (see Fokke, 1999). Threshold limits do not seem to exist for the removal of rather soft coatings. The removal rate should have a maximum at rather short relative exposure times (see Fig. 6.17). After a certain time, a further increase in exposure time reduces the removal rate.

Table 6.6 Removal kinetic power parameter, based on measurements from Raykowski et al. (2001) ($p = 0.35$ MPa, $\varphi = 90°$, $x = 38$ cm)

Abrasive type	Particle diameter in µm	n_t-value
Glass beads	125–177	0.56
	177–250	0.47
	420–590	0.47
Steel shot	90–200	0.51
	90–300	0.60

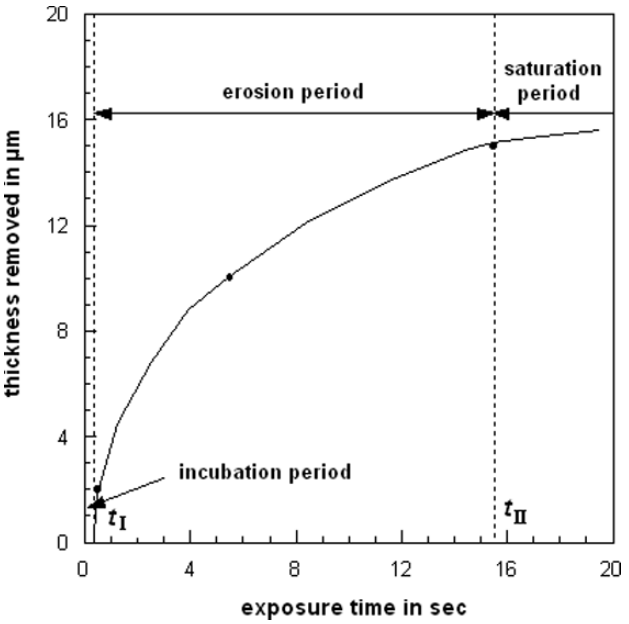

Fig. 6.17 Effect of local exposure time on the removal of a deposit from a turbine blade (based on results of Raykowski et al., 2001)

The qualitative relationship displayed in Fig. 6.17 corresponds well with measurements of area coverage values performed by Tosha and Iida (2001). The authors found an initial increase in the area coverage, which was followed by a saturation level at higher exposure times. Both ranges were separated by a "full coverage time". Coverage time increased if abrasive particle diameter increased, and if abrasive particle velocity decreased (see Sect. 3.5.4). This transition parameter may be close to the exposure time (t_{II}) defined in Fig. 6.17, which separates erosion period and saturation period. This time mark should not be exceeded in order to guarantee effective cleaning conditions. A similar transition parameter – the minimum number of impinging abrasive particles for the complete coverage of an area of 1 m^2 – was defined by Fokke (1999). This particular parameter mainly depended on the kinetic energy of the impinging particles (see Sect. 6.5).

6.3.5 Effects of Number of Passes

If the optimum exposure time, t_0, is known, a strategy for multi-pass material removal can be developed. The optimum exposure time can simply be introduced several times into the duration that corresponds to the desired volumetric removal rate. This approach delivers the following relationship:

$$n_S = \frac{\dot{V}_M}{\dot{V}_{M(t_E=t_O)}}; n_S = 1, 2, 3 \ldots \tag{6.15}$$

If, for example, a deposit with a thickness of $h_C = 16\,\mu m$ must be removed from a substrate, a local exposure time of $t_E = 20\,s$ is required. The optimum exposure time for $dh_C/dt_E = \max$ shall be $t_O = 2\,s$, which gives $h_C(t_E = t_0) = 6\,\mu m$. The theoretical number of steps calculated from (6.15) is $n_S = 16/6 = 2.67$. In practice, $n_S = 3$. The entire exposure time required to remove the desired coating mass is thus $t_E = 3.2 = 6\,s$ which is about 30% of the time for a one-step removal. The gain in efficiency is, therefore, as high as +70%. This example is based on Fig. 6.17.

6.4 Effects of Abrasive Parameters

6.4.1 Effects of Abrasive Mass Flow Rate

Effects of variations in abrasive mass flow rate on blast cleaning processes were investigated by Bae et al. (2007), Hareux and Riac (1986), Holt and Austin (2001) and Kura (2003). Figures 6.18 and 6.19 show typical relationships between abrasive mass flow rate and cleaning rate. Similar relationships were found for the removal of epoxy coatings from steel plates with steel grit (Bae et al., 2007); and for abrasive erosion of polyurethane and rubber (Zhang et al., 1995). The relationship can be expressed according to a reaction kinetics model (Momber, 1995):

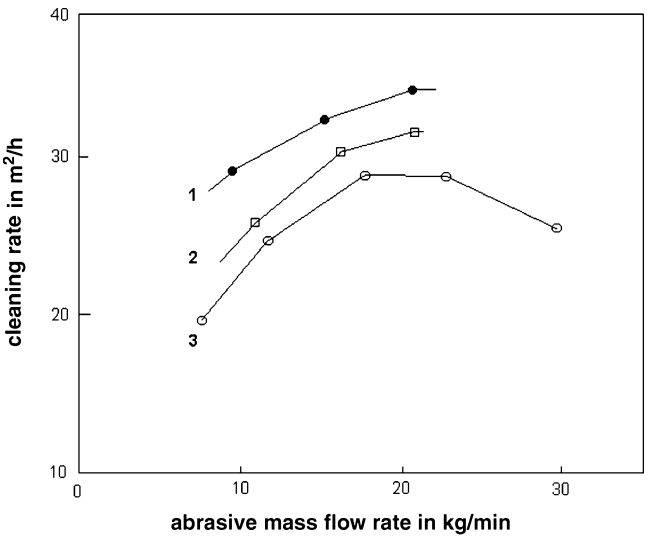

Fig. 6.18 Effect of abrasive mass flow rate on cleaning rate (Hareux and Riac, 1986). Abrasive material: aluminium oxide 700; nozzle types: 1 – long Laval nozzle, $d_N = 9.5$ mm; 2 – short Laval nozzle, $d_N = 9$ mm; 3 – cylindrical nozzle, $d_N = 10$ mm

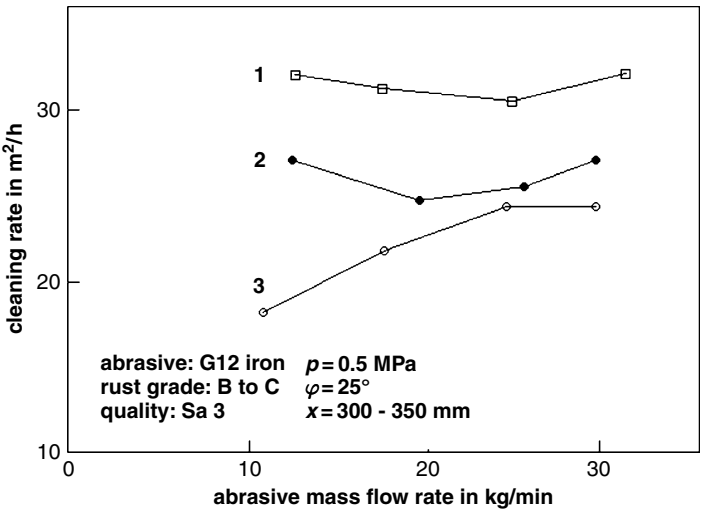

Fig. 6.19 Effect of abrasive mass flow rate on cleaning rate (Hareux and Riac, 1986). Abrasive material: iron shot G12; nozzle type: 1 – long Laval nozzle, $d_N = 9.5$ mm; 2 – cylindrical nozzle, $d_N = 10$ mm; 3 – short Laval nozzle, $d_N = 9$ mm

$$\dot{A} = k \cdot \dot{m}_P^m \tag{6.16}$$

In the equation, the power exponent, m, is a function of the abrasive mass flow rate. For small abrasive mass flow rates, $m = 1$. For the erosion of polymers, values between $m = 0.5$ and 1.0 were estimated (Zhang et al., 1995). For the slurry erosion of fusion-bonded epoxy powders, values between $m = 0.5$ and 0.6 were recorded (Luo et al., 2001). The value for m decreases up to $m = 0$ for optimum abrasive mass flow rates, and it becomes m ¡ 0 for high abrasive mass flow rates. From the point of view of abrasive consumption, the optimum range is at low abrasive mass flow rates and $m = 1$. In this range, each increase in abrasive mass flow rate leads to a proportional rise in the material removal rate. Such effects are known from abrasion tests of organic coatings, where mass loss linearly increases with the number of abrasion cycles (Cambruzzi et al., 2005). Fokke's (1999) erosive cleaning model also leads to a linear relationship between cleaning rate and abrasive mass flow rate (see Sect. 6.5). Results plotted in Figs. 6.18 and 6.19 show that an optimum mass flow rate depends on abrasive type and the nozzle configuration. It seems from the plot in Fig. 6.18, which is valid for aluminium oxide, that the optimum mass flow rate shifted to higher values if convergent–divergent nozzles ("1" and "2") were applied. For this nozzle type, the conditions for maximum cleaning rates were not yet reached. The cylindrical nozzle, however, featured a maximum cleaning rate at an abrasive mass flow rate of $\dot{m}_P = 17$ kg/min. For equal abrasive mass flow rates, the convergent–divergent nozzles generated a higher cleaning rate compared with the cylindrical nozzle. The advantage of the convergent–divergent nozzles seems to become even more pronounced at higher abrasive mass flow rates. The situation is

different in Fig. 6.19, which is valid for iron grit. In that case, only the curve for the short convergent–divergent nozzle (denoted "3") showed an optimum range for the abrasive mass flow rate. It was at about $\dot{m}_P = 25\,kg/min$. The other two nozzle types did not show any optimum range. In particular, the long convergent–divergent nozzle (denoted "1") was rather insensitive to changes in the abrasive mass flow rate. The cylindrical nozzle behaved completely different compared with the situation in Fig. 6.18. Whereas this nozzle exhibited an optimum performance at moderate values for the mass flow rate ($\dot{m}_P = 15$–$20\,kg/min$) in Fig. 6.18, it performed worst in that same abrasive mass flow rate range in Fig. 6.19.

The abrasive mass flow rate determines the number of impinging abrasive particles as well as their kinetic energies. The higher the abrasive mass flow rate, the higher the number of particles involved in the blast cleaning processes. Assuming no interaction between the individual abrasive particles in the course of acceleration, each increase in abrasive mass flow rate leads to a proportional increase in material removal. This holds for relatively low abrasive mass flow rates. It is known from wheel blasting, that a certain abrasive mass exists, which guarantees a complete coverage of a given surface with erosion pits. This critical abrasive mass is typical for a given substrate material, and it depends on abrasive material density and abrasive particle diameter (Safar, 1973). For rather high abrasive mass flow rates, damping mechanisms, particle collision, the generation of debris films and overlap effects may occur. Also, the limited kinetic energy of the air flow distributes over a very high number of particles, which leads to a decrease in the kinetic energy of the individual particles. This effect cancels the positive effect of the higher impact frequency. Figure 2.17 schematically illustrates these relationships. It is also known that an increase in the mass flow ratio abrasive/air reduces the velocity of the particles at the nozzle exit; this is true especially for smaller abrasive particles (see Sect. 3.6.2).

The location of the optimum abrasive mass flow rate depends on the deformation behaviour of the target materials. Whereas materials with the ability of plastic deformation reach the optimum at comparatively high abrasive mass flow rates; elastically responding materials reach the optimum region at lower abrasive mass flow rates. This difference is due to the higher sensitivity of brittle materials to the loading intensity provided by the abrasive particles. In contrast, a material responding with plastic deformation is more sensitive to the frequency of the impacting particles. Therefore, an increase in the abrasive mass flow rate is beneficial for these materials to overcome their plastic-deformation capability.

Experimental investigations have shown that the cleaning rate generally exhibited a maximum at an optimum number of turns on the abrasive metering valve (Holt and Austin, 2001; Kura, 2003; Bae et al., 2007). An example is shown in Fig. 6.20. It can be seen that the different abrasive materials responded differently to changes in the number of valve turns. The copper slag (denoted "1"), in particular, was very sensitive to changes in the number of turns. It can also be seen that the location of the maximum depended on the abrasive type. Each abrasive material is related to a certain number of turns (respectively to a certain cross-section of the valve opening). The optimum number of valve turns is six for the copper slag, and it is four for the

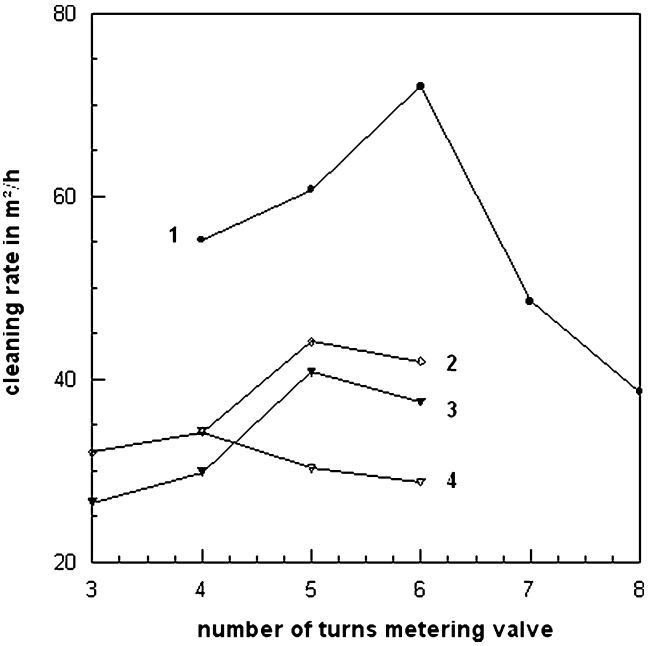

Fig. 6.20 Effect of abrasive metering on cleaning rate (Holt and Austin, 2001). Abrasive material: 1 – copper slag, 2 – hematite, 3 – garnet, 4 – coal slag

coal slag. It is conclusive that the specific abrasive consumption (in kg/m^2) must have a minimum value at that particular number of valve turns. It must, however, be taken into account that abrasive mass flow rate does not always have a linear relationship to the number of turns for all abrasive types. This was shown by Holt and Austin (2001). Therefore, the relationship between cleaning rate and abrasive mass flow rate does not always exhibit an optimum range (especially not for high air pressures), whereas the relationship between cleaning rate and number of valve turns always does.

Bae et al. (2007) published cleaning rates obtained during the removal of epoxy paint from steel substrate, whereby the values for the mass flow ratio abrasive/air were varied. The results depicted that cleaning rate decreased if the value for the mass flow ratio abrasive/air rose. The values for the mass flow ratio considered in this study ($R_m = 4$–4.4) were, however, unusually high.

Papini et al. (2003) defined a critical abrasive mass flow rate for significant inter-particle collision to occur. This critical parameter can be calculated as follows:

$$\dot{m}_C = \frac{4 \cdot \Pi_1 \cdot v_P \cdot \rho_P \cdot \pi \cdot r_P^3}{3 \cdot x} \tag{6.17}$$

The variable Π_1, a dimensionless mass flow rate, is given through the following equation (Papini et al., 2003):

$$\Pi_1 = \frac{\dot{N}_{P1} \cdot x}{v_P} \tag{6.18}$$

Here, the variable $\dot{N}_{P1}$ is a particle frequency at which significant interference (5%) between incident and rebounding particles begins to appear. It was found that this frequency depended, among others, on particle diameter and coefficient of restitution. Papini et al. (2003) performed numerical simulations to estimate values for Π_1 and found that this variable had low values for low x/d_P-ratios. The ratio x/d_P also determined the influence of the coefficient of restitution on Π_1. If the ratio was $x/d_P < 120$, Π_1 was high for high values for the coefficient of restitution; whereas the opposite trend was found for $x/d_P > 120$. Equation (6.17) can also be expressed in terms of the critical particle mass flux, passing through a nozzle:

$$\dot{m}_N = \frac{\dot{m}_C}{\pi \cdot r_N^2} \tag{6.19}$$

Parslow et al. (1997) performed erosion tests on enamel paints with a film thickness of DFT = 50 μm and found a relationship very similar to that plotted in Fig. 6.19. The authors utilised the abrasive concentration (g/m^3) as the evaluation parameter. At high values for the abrasive concentration, the erosion rate approximated a constant value in all cases. The value, where the erosion rate became stable, may be considered a typical parameter for a given paint material.

Walley and Field (1987) introduced an *incubation number* for the erosion of polymers. This number was defined as the number of impacts that have to occur on an impact zone before it contributes to a net mass loss. The incubation numbers were rather large for polymers, suggesting that the amount of deformation needed before material is removed was also large. This parameter had a strong relationship to the impact angle. If impact angle increased, the incubation number increased as well.

Glatzel and Brauer (1978) applied the *collision number* according to (2.12) to erosion processes, and they found that the mass loss decreased with an increase in the collision number according to the following relationship:

$$\Delta m_M \propto e^{-2 \cdot c_K} \tag{6.20}$$

6.4.2 Effects of Abrasive Flux Rate

Abrasive flux rate can be defined as follows:

$$\dot{m}_F = \frac{m_P \cdot \dot{N}_P}{A_C} \tag{6.21}$$

It expresses the mass of abrasive particles impinging a given cross-section during a defined time interval. Its physical unit is kg/(m^2 s). Flux rate, thus, can characterise

the impingement frequency. Detailed studies have shown that abrasive flux rate had comparatively little influence on the erosion of brittle materials and metals, but it was a sensitive parameter for the erosion of polymers and elastomers (Walley and Field, 1987; Arnold and Hutchings, 1989). Some results obtained on rubber are displayed in Fig. 6.21. It can be seen that erosion rate decreased as flux rate increased. The effects of varying flux rates were very pronounced in the range of small flux rates. The reasons for this behaviour were attributed to chemical degradation processes in the rubber material, and they were in detail discussed by Arnold and Hutchings (1989). The same trend was noted by Djurovic et al. (1999) for the removal of organic coatings from aluminium substrates with starch media. The authors found that cleaning efficiency dropped if specific abrasive consumption (kg/m^2) increased. Ciampini et al., 2003a) performed a simulation of the flux rate on abrasive particle interactions. They calculated critical values for the flux rate for negligible particle interactions. The critical value depended on the particle diameter. Typical values are listed in Table 6.7.

Henning and Brauer (1986) applied the frequency number according to (2.11), and they found an increase in the erosion rate with an increase in the particle frequency number. The progress of the erosion rate function did not depend on the material type; it had equal values for glass, aluminium, rubber and PMMA.

Hutchings (1981) derived a critical specific abrasive mass (kg/m^2) needed for the incubation of erosion processes in metals. This critical parameter was defined as follows:

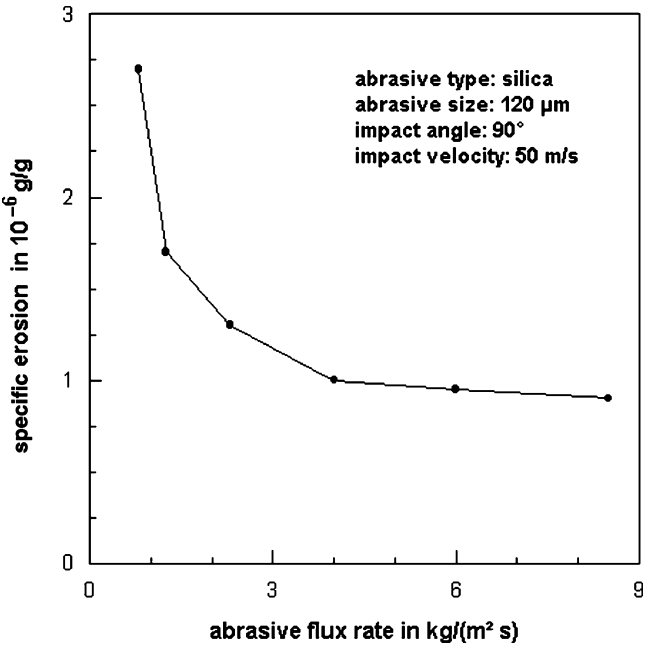

Fig. 6.21 Effect of abrasive flux rate on specific erosion in rubber (Arnold and Hutchings, 1989)

Table 6.7 Critical flux rates for negligible particle interactions (Ciampini et al., 2003a)

Particle diameter in µm	Critical flux rate in $kg/(s \cdot m^2)$
69	0.07
231	0.9
700	8.0

$$m_A \propto \varepsilon_C \cdot \frac{d_P}{v_P^2} \tag{6.22}$$

The power exponent for the particle velocity corresponded very well with experimentally estimated values (which were between 1.9 and 2.5 for aluminium). The parameter ε_C is a critical strain generated in the target material.

6.4.3 Effects of Abrasive Particle Diameter

Figure 6.22 illustrates a typical relationship between abrasive particle diameter and inverse cleaning rate for descaling. The time required to clean a given area was rather unaffected for small particle sizes. For particle diameters larger than $d_P = 1{,}000$ µm, cleaning time suddenly rose, and the descaling process became very inefficient. The relationship between cleaning rate and abrasive particle diameter can be characterised a follows:

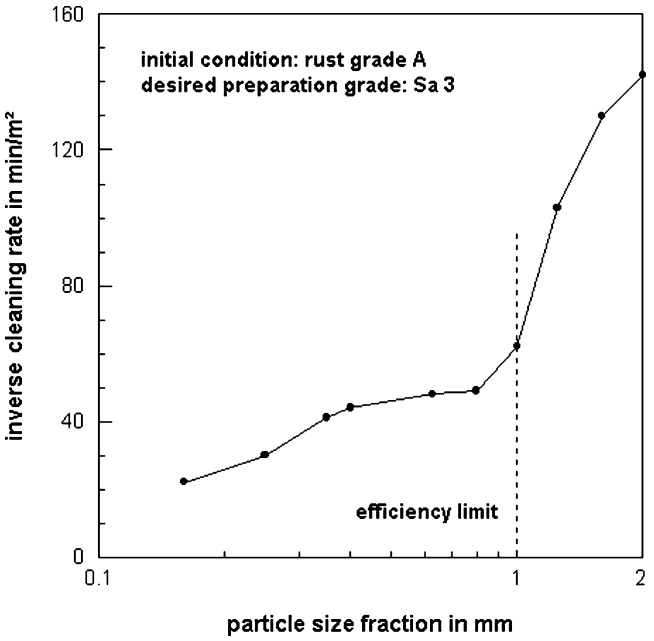

Fig. 6.22 Effect of abrasive particle size on inverse cleaning rate for mill scale (Neumann, 1976)

$$\dot{A} \propto d_P^{\theta_P} \tag{6.23a}$$

with $\theta_P < 0$.

It is important to note that the condition $\theta_P < 0$ holds for the relationship between particle size and cleaning rate as the target parameter. Figure 6.23 shows how a variation in abrasive particle size can be utilised for cleaning rate optimisation if a desired profile roughness must be realised. For a given roughness of $R_Z = 25$ µm, the specific rate varied between 60 min/m^2 (for $d_P = 1.0$ mm) and 130 min/m^2 (for $d_P = 1.6$ mm). This is a tremendous potential for cleaning process optimisation. The results plotted in Fig. 6.24 further verify the positive effect of smaller abrasive particles. For steel descaling, cleaning rate dropped for comparative mass flow rate values if larger abrasives were utilised. This effect is illustrated in Fig. 6.24a. The same trend between cleaning rate and abrasive particle size was reported by Bigos (1959) for the blast cleaning of steel panels with different abrasive materials (iron grit, sand and slag); by Balcar (1986) for the removal of bronze from steel substrates with glass beads; and by Bae et al. (2007) for the removal of epoxy coatings from steel substrates with steel grit. Results of the latter authors are provided in Fig. 6.24b. It can be seen that the relative cleaning rate notably dropped if larger abrasive particles were utilised for the removal of the epoxy primer. Figure 6.25 illustrates the effect of the abrasive size on the specific abrasive consumption. For comparative cleaning rates (about $\dot{A} = 30$ m^2/h), abrasive consumption was lowest for the smallest particle size and the lowest abrasive mass flow rate. Bullett and

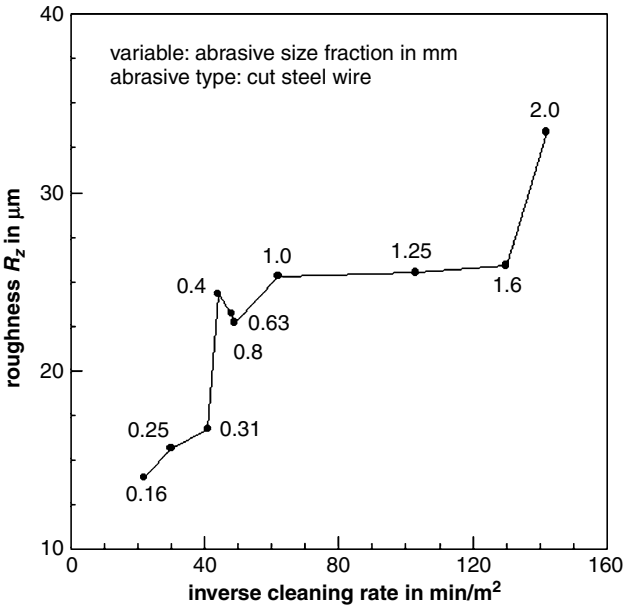

Fig. 6.23 Effects of final substrate roughness and abrasive particle size on inverse cleaning rate for mill scale (Neumann, 1976)

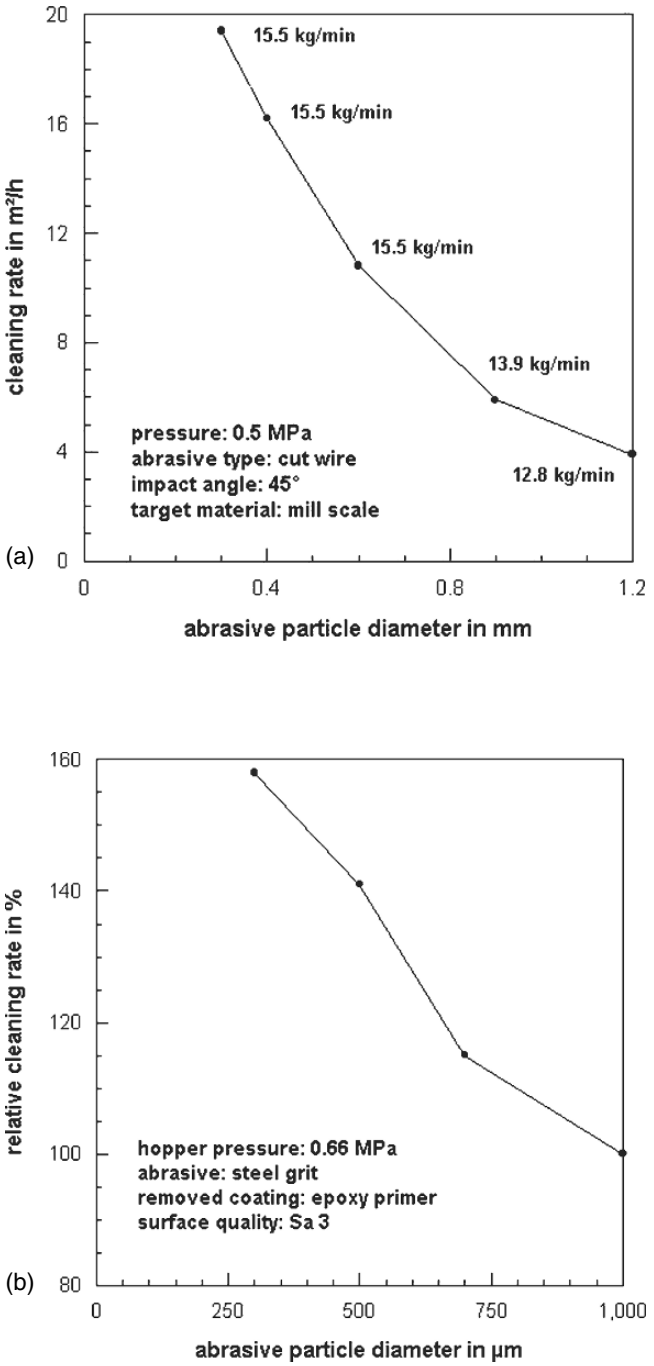

Fig. 6.24 Effect of abrasive particle size on cleaning rate. (**a**) Removal of mill scale (Remmelts, 1969); (**b**) Removal of epoxy primer (Bae et al., 2007)

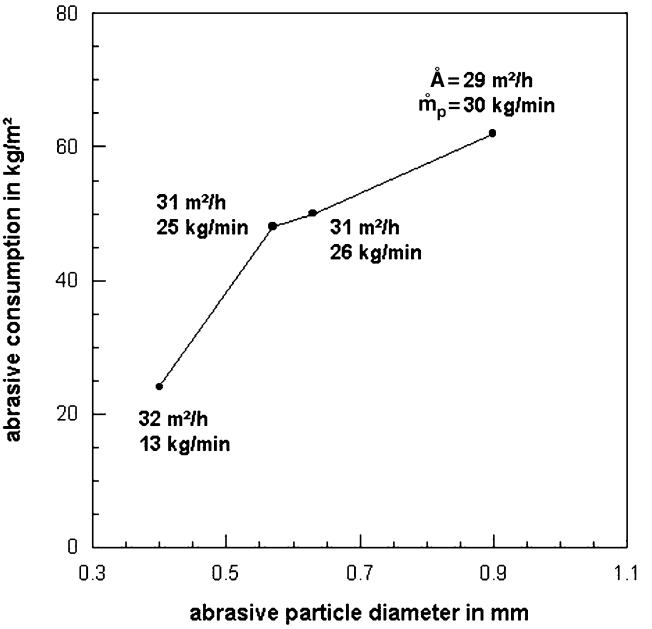

Fig. 6.25 Effects of abrasive particle size on specific abrasive consumption and cleaning rate (Hareux and Riac, 1986)

Dasgupta (1969) investigated the effect of abrasive size variation on the cleaning quality. They doped steel panels with ferrous sulphate and performed blast cleaning tests in order to remove this contaminant. Results of this study are displayed in Fig. 6.26 which reveals that a desired cleanliness (retained ferrous sulphate) could be achieved much earlier if smaller abrasive particles were utilised.

It seems, similar to the discussion in Sect. 6.3.3, that overlap and area coverage effects were important. Tosha and Iida (2001) have shown that the surface density of erosion dents in steel decreased with an increase in abrasive size according to a d_P^{-2}-relationship. Therefore, smaller particles guaranteed a closer coverage of the eroded surface. Smaller abrasive particle diameters also reduce the time where full area coverage starts [see (3.40)]. These findings support the recommendation in the SSPC Surface Preparation Commentary: "*Decreasing abrasive particle size can dramatically increase cleaning rate. The general rule is to use the smallest size abrasive that will do the job.*" Larger abrasive particle size may be beneficial for the removal of heavy coatings and scale.

Results of solid particle erosion tests on polymers and rubber are displayed in Fig. 6.27. Such stationary tests deliver different trends than cleaning tests with moving nozzles, because area coverage and overlap effects are not considered. The curves displayed in Fig. 6.27 can be subdivided into two sections: a linear section and a saturation section, whose locations depended on target material. On polyurethane, for example, the linear section was short, and there was some trend that a further increase in abrasive size would reduce erosion rate, similar to the situations shown in Fig. 6.24.

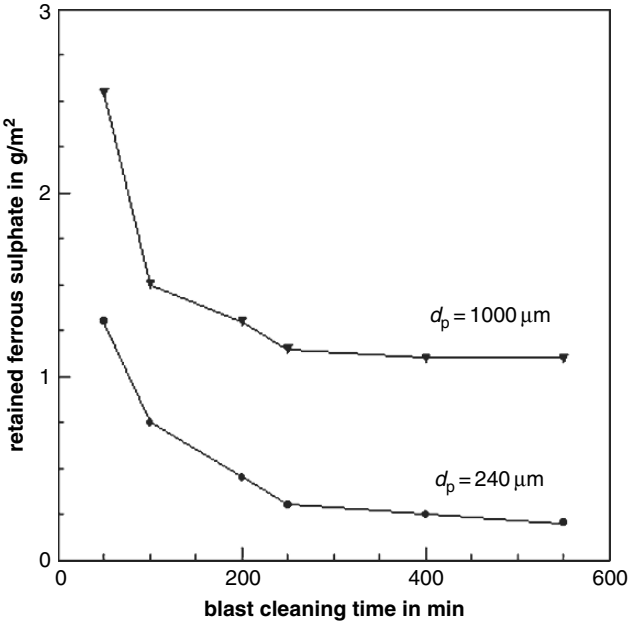

Fig. 6.26 Effect of abrasive particle size on substrate cleanliness (Bullett and Dasgupta, 1969)

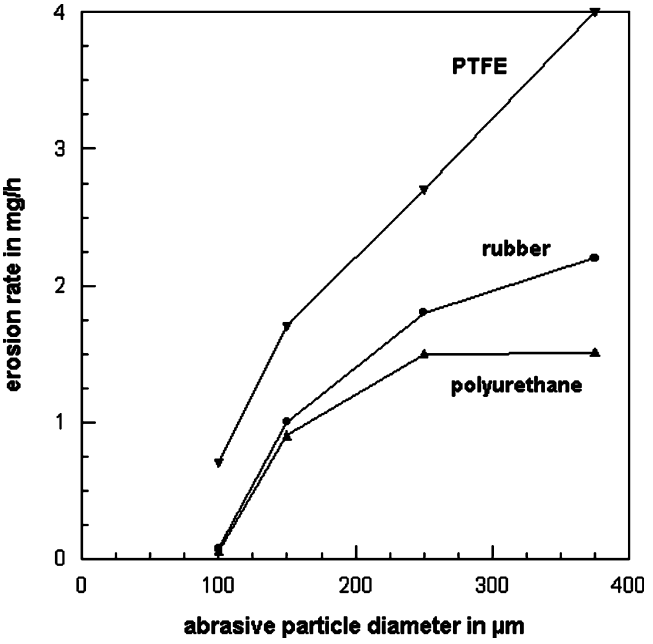

Fig. 6.27 Effect of abrasive particle size on the erosion of organic coatings (Zhang et al., 1995)

For the slurry erosion of fusion-bonded epoxy powder coatings, Luo et al. (2001) recorded two threshold particle diameters, a lower value ($d_P = 80$ µm) and an upper value ($d_P = 410$ µm), which enveloped the linear section. Beyond these two values, any notable particle size effects vanished. In the linear section, erosion rate increased linearly with increasing particle diameter. The reason for this relation was the higher kinetic energy of the larger particles as expressed by $E_P \propto d_P^{2.5}$. (Particle size affects abrasive particle velocity, which leads to a power exponent different from 3.) On the other hand, the number of impinging particles reduces with an increase in the particle diameter (see Sect. 2.6). In addition, abrasive particle velocity decreased if particle diameter increased, especially for low mass flow ratios abrasive/air (see Sect. 3.6.3). These effects became more important in the second range. In this range, the progress of the function dropped because of the reduced impact frequency and the reduced particle velocity. The optimum balance between the kinetic energy of a single abrasive grain and the number of impacting particles was exceeded.

The relationship between erosion rate and abrasive particle diameter can be approximated with a simple power law as:

$$E_R \propto d_P^{\theta_P} \tag{6.23b}$$

with $\theta_P > 0$.

In contrast to (6.23a), the power exponent has values larger than zero. If only the fundamental local material removal process is being considered, θ_P has always positive values. If, however, the cleaning process with a moving nozzle and notable particle interactions is considered, the condition $\theta_P < 0$ holds [see Fig. 6.24 and (6.23a)]. For rubber, the power exponent depends on the fatigue-function parameter: $\theta_P = \beta_F - 1$ (see Sect. 5.7.4 for the fatigue parameter β_F). Depth of both cracked layers and crack separation distance in eroded rubber surfaces increased nearly linearly with increasing particle diameter (Arnold and Hutchings, 1993). For polymers, values for the power exponent in (6.23) were between $\theta_P = 1.0$ and 2.0 (Zhang et al., 1995).

If the complete removal process, including overlap and superposition effects, is considered, values for θ_P may become negative as illustrated in Figs. 6.19a and 6.24 for mill-scale removal and coating removal applications.

Some other aspects that determine the influence of the abrasive particle diameter on the blast cleaning process are the higher impact fracture probability of larger grains (see Sect. 2.2.2) and the relationship between grain size and grain shape (see Sect. 2.3).

Bullett and Dasgupta (1969) investigated the effect of the abrasive particle size on the cleaning intensity. They contaminated rusty steel samples with a layer of ferrous sulphate and blast cleaned the samples with steel grit of two different abrasive sizes: a fine-grained abrasive ($d_P = 240$ µm) and a coarse-grained abrasive ($d_P = 1{,}000$ µm). The cleaning intensity was assessed based on the amount of retained ferrous sulphate after a given cleaning time. The results revealed that the application of the fine-grained abrasive materials led to much lower amounts of

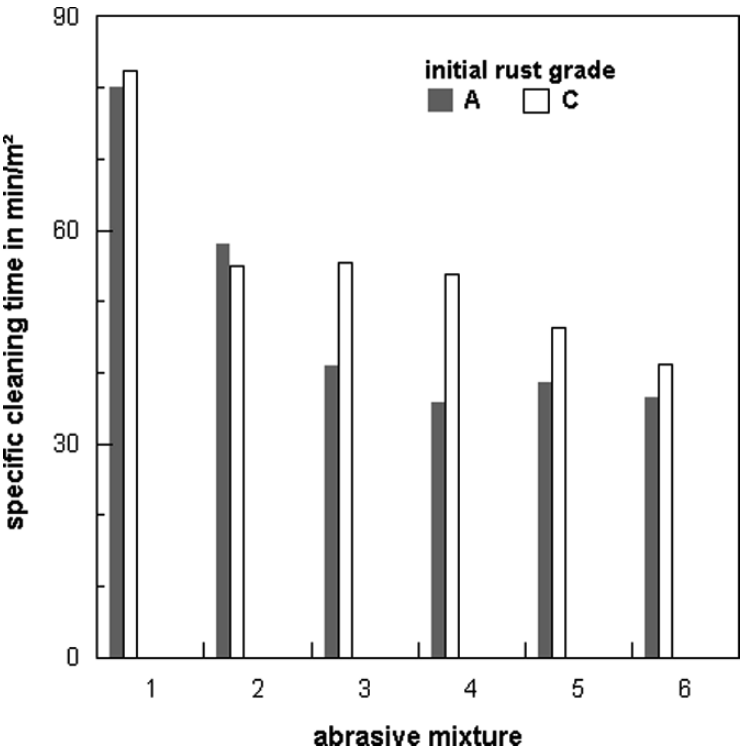

Fig. 6.28 Effects of abrasive mixture and initial cleaning condition on specific cleaning time (Neumann, 1976)

ferrous sulphate at all cleaning time levels. Therefore, an abrasive mixture with a high amount of small particles could guarantee a more thoroughly cleaned substrate.

The effect of abrasive working mixture on the cleaning of steel panels covered with mill scale (grade A), respectively rust (grade C), is illustrated in Fig. 6.28. The mixtures had different particle size class portions. The abrasive mixture "1" (coarse mixture, no grains smaller than $d_P = 315$ µm) could remove mill scale and rust with an equal efficiency, whereas the results for abrasive mixture "4" (medium mixture; no grains larger than $d_P = 1{,}250$ µm, no grains smaller than $d_P = 315$ µm) showed notable differences in the cleaning rates for the two types of oxide.

Safar (1973) defined a critical abrasive mass required for a complete coverage of the surface with erosion pits. For wheel-driven blasting machines, this critical abrasive mass can be approximated with the following relationship:

$$m_G = 2.09 \cdot \rho_P \cdot \left(\frac{d_P}{d_e}\right)^2 \cdot d_P \tag{6.24}$$

This equation should be applied to even surfaces only. It can be seen that the critical mass has a cubic relationship to the abrasive particle size. Table 6.8 lists

Table 6.8 Critical abrasive mass values for complete specimen coverage (Safar, 1973)

Target material	Abrasive diameter in mm			
	1.3	1.8	2.4	3.4
	Critical abrasive mass in kg/m^2			
Cast iron	143	198	265	375
Bronze	113	157	209	296
Carbon steel	107	148	198	281
Alloyed steel	102	141	189	266
Highly alloyed steel	121	167	224	317

experimental results, showing the effects of abrasive particle diameter and target material.

Peltzer (1955) gave some recommendations about the abrasive size for effective removal of mill scale (see Sect. 5.6.3) and cast sand from castings. Some of his recommendations are listed in Table 6.9.

6.4.4 Effects of Abrasive Particle Shape

Figures 6.29–6.31 show the effect of abrasive shape on the removal of organic coatings. Figure 6.29 deals with the removal of baking enamel from different metal substrates. The use of spherical steel particles led to lower cleaning rates compared with the angular grit particles. This effect was most pronounced for the aluminium substrate, where grit particles (angular shape) were much more efficient than shot particles (rounded shape). For a stainless steel substrate, in contrast, particle shape did not affect the coating removal efficiency. Figure 6.30 illustrates some effects of coating composition. All coatings were more sensitive to the impingement of steel balls compared to the impingement of a cone-shaped particle. It can also be seen that the size of the ball played an additional role. Figure 6.31 shows the effects of particle shape and target material hardness. Grit particles were more effective at both target hardness levels, although the differences in specific volume loss were sensitive to the target material hardness. For the lower target hardness value, particle shape had a pronounced influence on the specific volume loss, whereas only a weak effect was found for the higher target hardness value. Irregular particles may, therefore, be recommended for the removal of rather soft materials. For rubber, impinged at

Table 6.9 Particle size recommendations for the removal of cast sand from castings (Peltzer, 1955)

Casting type	Recommended abrasive size	
	Shot	Grit
Iron casting	S 550–S 320	G 16–G 40
Annealed casting	S 550–S 330	G 18–G 40
Steel casting	S 660–S 390	G 14–G 25

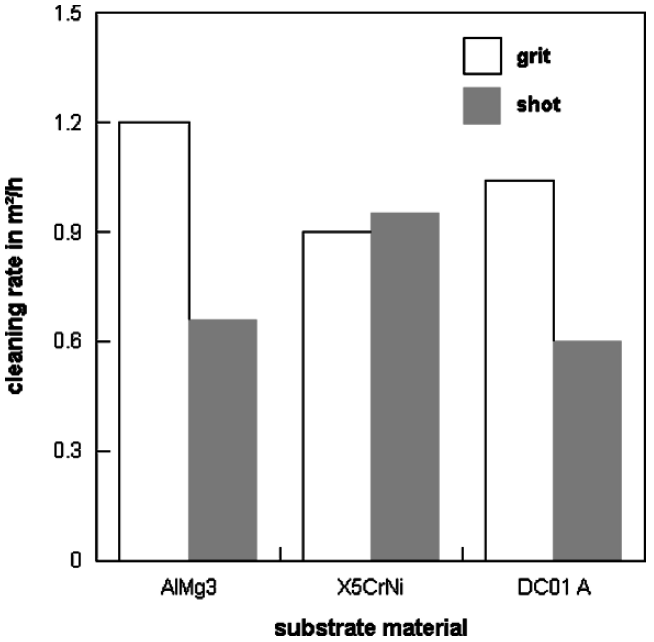

Fig. 6.29 Effect of particle shape on the cleaning rate for baked enamel (Uhlmann et al., 2003)

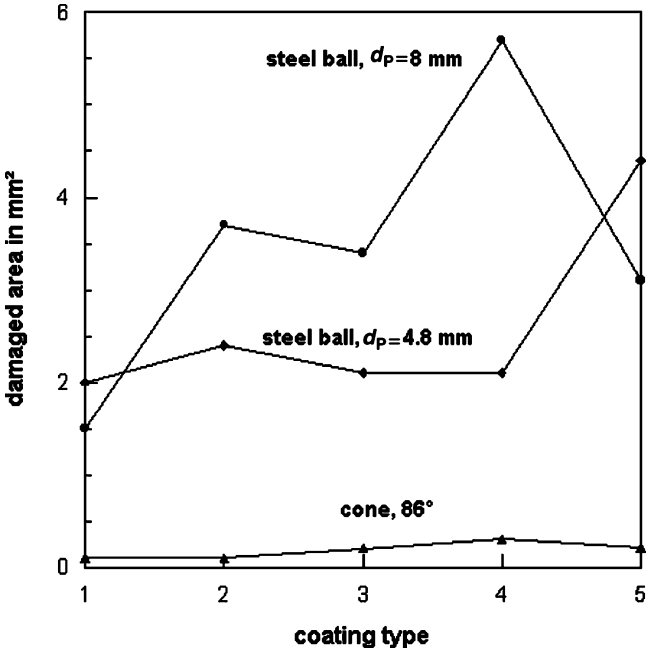

Fig. 6.30 Effect of particle shape on the damage size in different coating types (Breinsberger and Koppelmann, 1982). Coating types: 1-DFT = 72 µm, 150/140 °C; 2-DFT = 77 µm, 120/140 °C; 3-DFT = 78 µm, 160/140 °C; 4-DFT = 78 µm, 160/140 °C; 5-DFT = 80 µm, 160/140 °C

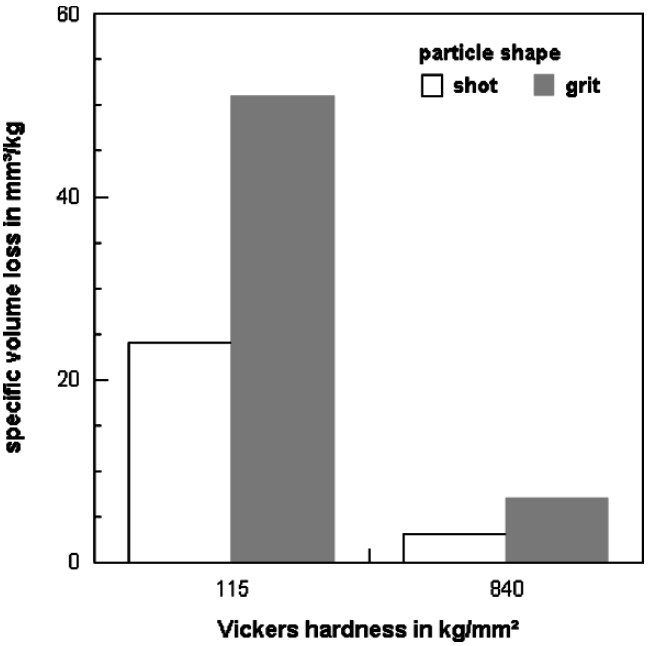

Fig. 6.31 Effects of particle shape and target material hardness on the specific volume loss in steel targets (Wellinger and Uetz, 1955)

oblique impact angles, erosion rate increased substantially for more angular particles (Arnold and Hutchings, 1992).

Basically, these findings support the recommendation given in the SSPC Surface Preparation Commentary: "*Rounded particles are most effective in removing brittle coatings such as mill scale, whereas angular shaped particles are more effective in removing softer coatings such as rust and paint.*"

Systematic studies in the field of solid particle erosion have shown that the abrasive grain shape had an important influence on the material removal regime. Bahadur and Badruddin (1990) related the particle shape influence to the different removal mechanisms, such as micro-cutting for angular particles and micro-ploughing for spherical particles. Cousens and Hutchings (1983) showed that the usually used terms 'ductile' and 'brittle' behaviour are determined by the abrasive grain shape.

Abrasive particle shape also effects the acceleration of the particles in the blast nozzle (see Sect. 3.6.4). Grit particles tend to have higher velocities than shot particles.

6.4.5 Effects of Abrasive Material Hardness

From investigations of abrasion and solid particle erosion is known that a "transition stage" exists at the point of comparable hardness of abrasive material and target material (Wellinger and Uetz, 1955; Uetz, 1986):

$$\frac{H_M}{H_P} \rightarrow 1.0 \text{ to } 1.5 \tag{6.25}$$

In this region, erosive material removal processes are very sensitive to changes in the relative hardness. Figure 6.32 illustrates these relationships. For the substrate with the high hardness ($H_M = 440\,kg/mm^2$), the specific mass loss exhibited a high increase if the abrasive hardness exceeded a value of $H_P = 500\,kg/mm^2$. The corresponding hardness ratio was about $H_M/H_P = 0.9$, which agrees very well with (6.25). For the substrate with the lowest hardness, the progress of the function dropped with an increase in the abrasive material hardness. Beyond a critical hardness ratio between abrasive and target material (at about $H_P/H_M = 2.4$), the progresses of the functions exhibited a steep decrease. Any further increase in the abrasive hardness would not substantially improve the material removal performance. A general rule in the SSPC Surface Preparation Commentary is: "*Select the minimum abrasive hardness that will effectively do the job.*"

Figure 6.33 illustrates the effects of abrasive material hardness on the erosion of rubber. In contrast to Fig. 6.32, there is no unique trend visible in the graph. The maximum specific volume loss occurred at rather low abrasive hardness values ($H_P = 500$–$900\,kg/mm^2$) and not, as could have been expected, at the highest value for the abrasive material hardness. These relationships were contributed to abrasive particle shape effects. The glass and flint particles were characterised by pronounced edges, and they basically removed material due to micro-cutting. For rubber, as a soft material, this erosion mode contributed to high levels of material

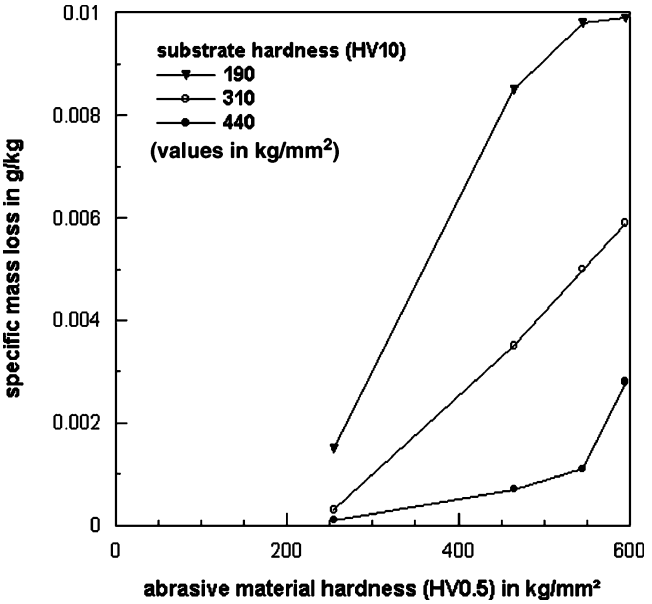

Fig. 6.32 Effect of abrasive material hardness on specific mass removal (Wellinger and Gommel, 1967). Process parameters: abrasive type: cut steel wire; $d_P = 400\,\mu m$; $v_P = 70\,m/s$

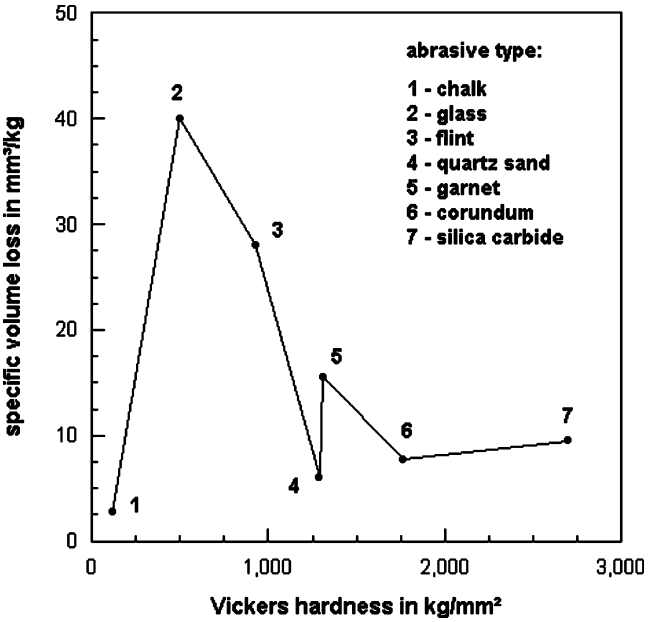

Fig. 6.33 Effect of abrasive material hardness on specific volume loss in rubber (Wellinger and Uetz, 1955)

removal. Particle shape was, therefore, much more important to the rubber material than abrasive material hardness.

Wellinger et al. (1962) investigated the effects of tensile strength of abrasive materials (cut steel wire) on the specific material loss of steel target and found a relationship very similar to that shown in Fig. 6.32. The authors found that the influence of the abrasive material tensile strength vanished for very high values of target material hardness.

6.5 Removal Models

Rosenberger (1939) probably provided the first, simple material removal model for blast cleaning processes whereby the material removal due to the impingement of an individual abrasive particle was considered a machining process.

Fokke (1999) developed a model for the estimation of the cleaning efficiency for the removal of organic coatings from steel substrates due to blast cleaning. The model is based on a geometric description of the coating area removed during the impingement of an individual abrasive particle. Fokke (1999) obtained this area due to precise surveys of impact craters.

For a chosen kinetic energy of a particle (see Sect. 2.6.2 for additional information), a minimum number of particles, which is required to erode an impacted area of 1 m^2, can be computed as follows:

$$N_{P\,min} = \frac{1}{\varepsilon_M \cdot E_P} \tag{6.26}$$

The number is a minimum because its establishment assumes that the impact areas of all particles do not overlap. The physical unit of the minimum number is m^{-2}. The parameter ε_M was experimentally estimated by Fokke (1999); an example is provided in Fig. 6.6. Typical values were between $\varepsilon_M = 2.6 \times 10^{-5}$ and 2.9×10^{-5} m^2/J; they depended on coating hardness and abrasive particle size. A dimensional analysis of the size of craters formed in the coating as a result of particle impingement delivered the following relationship:

$$\frac{V_C}{d_P^3} = \Psi_M \cdot \left(\frac{E_P}{H_M \cdot d_P^3}\right)^{1.5} \tag{6.27}$$

The parameter ψ_M is a dimensionless scaling parameter. For a given coating material (given coating hardness), this relationship can be simplified as follows:

$$V_C = \Psi_N \cdot E_P^{1.5} \cdot d_P^{1.5} \tag{6.28}$$

The parameter ψ_N is an empirical parameter with the unit ($m^{4.5}/J^{1.5}$). If the abrasive particle size is known, values for ψ_N can be estimated due to linear regressions of experimental results as presented in Fig. 6.6. When a number of particles each remove a volume V_C from $1\,m^2$ of substrate, the coating layer is reduced by an average thickness Δh_C, the total number of impacts required to totally remove the coating down to the substrate, reads as follows:

$$N_P \cdot N_{P\,min} = \frac{n_C}{V_C} \tag{6.29}$$

For a given particle diameter, the number of particles impinging a given area depends on abrasive mass flow rate and traverse speed. The traverse speed can be expressed by the cleaning rate because this parameter is nothing else than an area traversed during a given time period. This reflection leads to the following equation:

$$\dot{A} = \frac{\dot{m}_P}{N_P \cdot N_{P\,min} \cdot V_P \cdot \rho_C} \tag{6.30}$$

The linear relationship between cleaning rate and abrasive mass flow rate corresponds well with the results provided in Sect. 6.4.1 for small and moderate abrasive mass flow rates. The inverse relationship between cleaning rate and abrasive particle size also verifies experimental results obtained on mill scale and soft coatings (see Sect. 6.4.3). It is also conclusive that cleaning rate may reduce for coating materials with higher density values.

Uferer (1992) derived an empirical model for the removal of mill scale and rust from steel substrates. The final equation reads as follows:

Table 6.10 Constants for the model of Kambham et al. (2006)

Constant	*a*	*b*	*c*	*d*	*e*	*f*
Value for rusted panels	−129.40	9,405.97	2,943.53	−235, 051.25	−12, 593.40	−16, 946.26
Value for painted panels	542.45	−67, 478.23	−806.87	3,532,289.80	10,379.03	−145, 564.76

Table 6.11 Variable range for the model of Kambham et al. (2006)

Variable	Unit	Range
Air pressure	psi	80–120
Abrasive mass flow rate	lbs/min	8–26

$$A_S = \frac{\dot{A}}{\dot{m}_P} = (K_0 \cdot K_1 \cdot \dot{m}_P - a_0 \cdot K_1^2 \cdot \dot{m}_P^2) \cdot f_P \cdot f_N \cdot f_X \cdot f_\phi \tag{6.31}$$

The parameter A_S is the specific cleaning rate in m^2/kg; it is actually the inverse version of (6.5). Values for the parameter constants f_N, f_X and f_ϕ are provided in Tables 6.3–6.5. The constants K_0, K_1 and α_0 must be established due to a standard blast cleaning test. Uferer (1992) recommended the following parameter configuration for such a standard test: $p = 0.25\,\text{MPa}$, $x = 50\,\text{cm}$ and $\varphi = 90^\circ$.

Kambham et al. (2006) issued a model for the removal of rust and coatings from steel substrates due to dry blast cleaning. The model is based on regression statistics. The authors performed numerous blast cleaning trials and applied a standard data-fit method. The final equation reads as follows:

$$\dot{A} = a + \frac{b}{p} + \frac{c}{\dot{m}_P} + \frac{d}{p^2} + \frac{e}{\dot{m}_P^2} + \frac{f}{p \cdot \dot{m}_P} \tag{6.32}$$

The cleaning rate is given in ft^2/h. The regression parameters a to f for the two removal modes "rust" and "coating" are listed in Table 6.10. Table 6.11 lists the parameter ranges for the two process variables. Because the regression coefficients are in the range of about 0.6 only, the use of the model may be restricted to the determination of qualitative trends only. Another limit of the model is its restriction to coal slag as an abrasive material.

6.6 Efficiency of Blast Cleaning

6.6.1 Erosion Efficiency

The efficiency of the erosion process is difficult to evaluate. Following Thiruvengadam's (1967) erosion resistance model (which is, rigorously taken, valid

for liquid drop impact), a probable approach involves the strain energy density defined in (5.2). This parameter characterises the amount of energy stored in a stressed volume. If this parameter is being related to the specific material removal energy, the efficiency can be approximated as follows:

$$\Phi_{\mathrm{E}} = \frac{\mathrm{E_{SD}}}{\mathrm{E_{sp}}} \cdot 100 \tag{6.33}$$

The specific energy is given through $E_{\mathrm{P}}/V_{\mathrm{M}}$. From Fig. 6.6, respectively (6.11), one obtains $E_{\mathrm{sp}} \propto E_{\mathrm{P}}^{-1/2}$. A particle with a kinetic energy of 10 mJ removes a paint volume of 10^{-11} m^3 (see Fig. 6.6), which results in a specific energy of $E_{\mathrm{sp}} = 10^3$ MJ/m^3. A typical value for the elastic strain energy density of an organic paint is $E_{\mathrm{SD}} = 5$ MJ/m^3 from Table 5.6. For these numbers, (6.33) delivers a material removal efficiency of $\Phi_{\mathrm{E}} = 0.5\%$. If additional energy dissipation due to plastic deformations is assumed, an erosion efficiency of about 1% is an approximate value. This order of magnitude corresponds with results from calculations for hydro-abrasive erosion of steel (Momber et al., 1996). Mineral grinding processes also have a mechanical efficiency in the range of one percent only (Schubert, 1988).

6.6.2 General Aspects of Process Efficiency

Numerous factors affect the efficiency of blast cleaning processes. Experience show that the most important factors are the following:

(1) existing coating type, adhesion and condition;
(2) substrate material properties;
(3) experience and organisation of the working crew;
(4) geometry and accessibility of the objects.

The aspects (1) and (2) are considered for shipyard operations in a benchmarking report (Appleman et al., 1998).

The criterion “existing coatings” is treated in terms of “type of surface” and “coating hardness”, whereas the latter term basically characterises the resistance of the coatings against the action of impinging abrasive particles during blast cleaning. In terms of “type of surface”, four categories are being distinguished:

- Light rust, light mill scale or loose paint: This is a deteriorated surface which requires little effort to clean.
- Tight rust or tight mill scale: This is new structural steel from the mill.
- Thin paint or rusted thin paint: This is previously coated steel plate where the coating thickness is in the range of DFT = 120 to 175 µm.
- Thick paint, heavy mill scale, or heavily pitted rust: This can be steel plate where the coating thickness in the range of, or greater than, DFT = 200 to 250 µm.

In terms of “coating hardness”, the report distinguished between the following three categories:

- hard coatings: typically chemically cured coatings (epoxy, urethane, zinc-filled coatings);
- soft coatings: typically a more readily deformed surface (alkyd, latex, chlorinated rubber);
- no coating: new mill scale bearing steel.

Numerous remarks on the effects of mechanical properties of coatings on the erosion process are delivered in Chap. 5.8. A further example is shown in Fig. 6.34. The graph illustrates the effect of the target material (e.g. metallic coating) on the specific erosion. It can be seen that specific erosion increased notably in the range of low hardness values. If the hardness was rather high, it did not affect the erosion process. These results correspond to the relationships discussed in Sect. 6.4.5. An additional point of interest, however, is the effect of the air pressure on the erosion of the target material. Pressure effects were very pronounced in the range of low hardness values. However, for higher values of target hardness ($H_M > 700\,kg/mm^2$), the gain of the higher pressure seemed to vanish.

The aspect (3) is illustrated in ISO 12944-4, which states the following: "*Personnel carrying out surface preparation work shall have... sufficient technical knowledge of the processes involved.*" This includes knowledge about the equipment being used, the basic principles of blast cleaning and the effects of major process parameters. Health and safety training is another important issue of personnel qualification. Experience shows that trained blasters can outperform untrained blasters by a factor

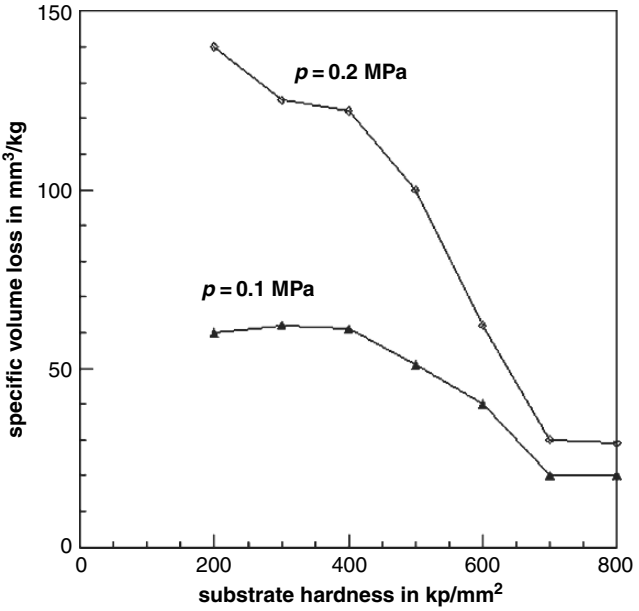

Fig. 6.34 Effect of substrate hardness and air pressure on specific volume loss in metal (Gommel, 1967a)

of about two. Training and qualification counts even more if high-level surface preparation operations are being performed, which would include, among others, the treatment of stainless steel, tank coating surface preparation, or the preparation of substrates for metal-sprayed coatings.

Regarding aspect (4), a detailed investigation has shown that accessibility can dramatically affect efficiency as well as quality of blast cleaning. For steel bridge structures with delicate geometry, only 25–30% of the interior limited access surface could be cleaned by blast cleaning. Also, profile depth was only 85% of the values generated during normal blast cleaning procedures (Bullard et al., 2002). Some results are listed in Table 6.12. Based on the data, blast cleaning inside gap widths of 0.3–0.6 cm on 10-cm-deep back-to-back angles did not reach approximately 50–75% of the total angle depth. That is, only 25–50% of the interior surface was being cleaned. For 5-cm-deep back-to-back angles, 25–50% remained uncleaned, while 50–75% was prepared. Blast cleaning penetration increased when gaps were 1.2 cm and wider, but was also somewhat dependent on angle depth. Cleaning rate also depends on work location. Examples from the ship building industry are listed in Table 6.13. It can be seen that cleaning rate can drop up to 75% for very complex structural shapes.

6.6.3 Aspects of Site Management

Site management has a notable effect on efficiency especially if site environment is not a stable factor in blast cleaning. Here, experience is again an issue. However, other problems are of importance as well, namely the following (related basically to external site applications):

- Work delay occurs while operators are waiting for broken equipment to be repaired.
- Preventive maintenance is being performed during the blast shift and subsequently displaces operators who would be blasting regularly.
- Relocating a compressor or a blast machine is often a timely process. The technician must evaluate the desired location of the unit, search for a suitable power source and obtain the connecting cables before work can continue. Hose lines must also be replaced.

Table 6.12 Abrasive blast penetration at typical difficult-to-access areas (Bullard et al., 2002)

Gap width in cm	Depth cleaned in cm		Area cleaned in %	
	10 cm angle	5 cm angle	10 cm angle	5 cm angle
0.31	2.38	2.40	24	48
0.66	4.60	3.50	46	70
1.25	4.48	5.00	45	100
1.88	9.15	5.00	92	100
2.50	9.63	5.00	96	100

Table 6.13 Cleaning rates modifications due to work location in the ship building industry (NSRP, 1998b)

Location	Relative cleaning rate in %
Hull section; easily reached	100
Complex steel shape; less than 8.25 m elevation	75
Hull section; 8.6–25 m high	75
Complex steel; 8.6–25 m high	75
Hull section; 26–50 m high	50
Complex steel; 26–50 m high	50
Interior tank spaces; little structural steel	50
Interior tank spaces; complex structural shapes	25

- Electrical outages and power supply problems disrupt entire teams during operation. When electrical services on the site are interrupted, qualified technicians must be utilised to restart the units.
- Lack of hose management causes significant delay time, especially if long distances between compressor and blast machine, respectively between blast machine and nozzle, need to be bridged.
- Dressing and inspecting personal protective equipment is a time-consuming function of the manual operator.
- Cranes are often unable to make lifts at night due to poor lighting. Therefore, compressors, abrasive hoppers and other equipment cannot be moved at appropriate speed.

6.6.4 Aspects of Operators' Fatigue

A further aspect that affects efficiency is operator fatigue, especially if the equipment is run manually. Typical problems associated with fatigue can be summarised as follows:

- The grit hoses are supported partly by the operator as he works. Both the weight of the hose and the pull from horizontal friction increase the fatigue. Fatigue increases if hose diameter increases. Wipe hoses are, therefore, frequently used.
- The weight of the nozzle is fatiguing to the operator; this weight is completely supported by the arms and neck of the operator.
- In order to reach surfaces behind obstructions, an operator is forced to position his nozzle in awkward angles. This strain is magnified if the operator stands in a basket on a high-reach.
- While blasting overhead in areas with low clearance, the operator is often forced to a squatting position to blast; this directs forces to the knees.
- Working in overhead areas with tall clearances, the operators are often forced to reach overhead with the nozzle to make contact with the surface. This compounds forces in the elbows and shoulders.
- Operators are often uncomfortable due to dust.

- Operators are often uncomfortable due to cumbersome personal protective equipment.
- Operators often have their vision obstructed by dirty safety glasses.
- Operators often have their vision impaired by poor lighting at night.
- Operators often do not practice sound ergonomic principles as they confirm their duties.
- Operator's efficiency decreases in productivity as their shift progresses. Even after standard breaks, production at the end of the shift is significantly less than at the beginning.

A major conclusion drawn from these observations is the performance of ergonomic training (which may be done by contractors) and the development of ergonomic support devices (which may be done by manufacturers).

Fatigue due to the jet flow reaction force can be approximated as follows:

$$\mathrm{F_R} = \dot{\mathrm{m}}_\mathrm{A} \cdot \mathrm{v_A} + \dot{\mathrm{m}}_\mathrm{P} \cdot \mathrm{v_P} \tag{6.34}$$

It can be seen that an efficient nozzle, which delivers high exit velocities for air and abrasive particles, is associated with an increase in fatigue. The same is true for the use of large-diameter nozzles, which allow for high air and abrasive mass flow rates. If typical values from Chap. 2.6 are taken ($\dot{m}_\mathrm{A} = 10\,\mathrm{kg/min}$, $\dot{m}_\mathrm{P} = 15\,\mathrm{kg/min}$, $v_\mathrm{A} = 500\,\mathrm{m/s}$ and $v_\mathrm{P} = 180\,\mathrm{m/s}$), a corresponding reaction force of $F_\mathrm{R} = 130\,\mathrm{N}$ can be calculated. The reaction forces generated by a blast cleaning nozzle flow were measured by Kline et al. (1988) for different nozzle designs, and values between $F_\mathrm{R} = 49$ and $67\,\mathrm{N}$ were estimated experimentally. These results are notably lower than the calculated value, which is most probably due to impulse losses during the acceleration process and the flow of the jet through the surrounding air. Therefore, (6.34) delivers rather overestimated values in terms of reaction force assessment. Rosenberg et al. (2006) developed a biomechanical model for the approximation of hand forces and wrist moments. For blast cleaning with steel shot, they reported force values of $F_\mathrm{R} = 26\,\mathrm{N}$ at the hand, and moment values of 3 Nm at the wrist.

Critical, respectively permissible, reaction force values do not exist by law for blast cleaning applications. For hydroblasting applications, however, such permissible limits exist, and they may be applied for comparative purposes (Momber, 2003, 2005a). For the operation of hand-held water jet guns, the permissible limit is, for example, at $F_\mathrm{R} = 150\,\mathrm{N}$, which is more than three times higher than the values measured for dry blast cleaning. Another parameter which helps to assess the severity of fatigue due to the jet flow reaction force is the weight of the operator. Experience from water jetting applications shows that a gun can be handled in a safe and efficient way if the reaction force of the jet does not exceed one-third of the weight force of the operator. The weight force of an operator (blaster) is simply:

$$\mathrm{F_W} = 9.81 \cdot \mathrm{m_O} \tag{6.35}$$

whereby the weight of the operator is given in kg. The fatigue condition is then:

$$\frac{F_W}{3} > F_R \tag{6.36}$$

The weight force of a 75-kg operator, for example, is $F_W = 735\,N$; one-third of this value is $F_R = 245\,N$, which again is much higher than typical values estimated for blast cleaning.

6.7 Weld Seam Cleaning

Experimental results of weld seam cleaning with different treatment methods were reported by Remmelts (1969) and Blomquist (1997). Some results are summarised in Table 6.14. It can be seen that the proper selection of the abrasive type can have a considerable effect on the cleaning rate. The cleaning rate was high for crystal grit and rather low for steel grit. Vacublast and manual grinding resulted in very low cleaning rates.

Remmelts (1969) investigated the effects of weld type, abrasive size and abrasive mass flow rate in more detail. Results of his study are provided in Table 6.15. The results verify the higher cleaning capability of non-metallic abrasive materials. Cleaning speed was higher and specific abrasive consumption was lower if copper slag was used instead of cut steel wire.

Table 6.14 Cleaning rates for weld seam cleaning (Blomquist, 1997)

Method	Weld seam length in m	Cleaning speed in m/min
Blast cleaning with steel grit	115	1.3
Blast cleaning with aluminium oxide	67	2.1
Blast cleaning with crystal grit	50	2.3
Manual grinding	14	0.03
Vacublast	4	0.93

Table 6.15 Cleaning speeds for weld seam cleaning (Remmelts, 1969). Parameters: $p = 0.5\,MPa$, $d_N = 10\,mm$, $x = 56\,cm$; ship plate (12 mm), arc welding

Type of weld	Abrasive type	Abrasive size in µm	Abrasive mass flow rate in kg/min	Cleaning speed in m/h	Abrasive consumption in kg/m
Butt weld	Cut wire	400	18.7	270	4.2
		900	16.4	135	7.3
	Copper slag	900	5.7	180	1.9
Fillet weld (vertical)	Cut wire	400	18.7	108	10.4
	Copper slag	400	8.9	126	4.3
Fillet weld (flat)	Cut wire	400	18.7	101	11.1
	Copper slag	400	8.9	119	4.5

6.8 Underwater Applications

Blast cleaning can be performed under submerged conditions. Typical applications would include the cleaning of steel piles prior thickness measurements, the cleaning of submerged constructions for inspections and the removal of rust and deteriorated coating systems. However, just a few systematic investigations about the efficiency of submerged blast cleaning applications have been performed. Donker (1985) and Donker and Richter, (1982, 1988) conducted a number of tests at water depths between 10 and 50 m with a special adapter in front of a standard blast cleaning nozzle. This adapter created an air shroud between nozzle exit and target surface. A special bypass-control avoided the penetration of water into the grit hose and kept the abrasive material dry. The experimental conditions are listed in Table 6.16, and results are provided in Table 6.17. The cleaning rate of up to $\dot{A} = 7\,\mathrm{m^2/h}$ was high and comparable to cleaning rates for atmospheric blast cleaning. The authors found, however, that cleaning rate depended on initial surface condition (see Fig. 6.35a). The values for the specific abrasive consumption, provided in Fig. 6.35b, were notably higher than values for atmospheric blast cleaning, and they also depended on the initial condition. Tar epoxy was the most difficult to remove material.

A very special submerged application is "blast zincing" (Groot et al., 1982; Donker and Richter, 1988). In that application, zinc-coated abrasive particles are used as a blasting media, and the particles, either being embedded in the steel substrate or forming a protective layer on the steel surface, are considered to act as sacrificial anodes. The idea is illustrated in Fig. 6.36. Typical performance data for blast zincing is an efficiency of $\dot{A} = 3\,\mathrm{m^2/h}$ and a specific abrasive consumption of $\dot{m}_S = 112\,\mathrm{kg/m^2}$ (Donker and Richter, 1988).

Table 6.16 Experimental conditions for underwater blast cleaning tests for water depths up to 30 m (Donker and Richter, (1982)

Parameter	Value
Nozzle type	Laval nozzle
Nozzle diameter	10 mm
Grit hose diameter	32 mm
Air pressure	0.8 MPa
Air volumetric flow rate	$10\,\mathrm{m^3/min}$
Abrasive type	Quartz sand
Abrasive size	1.0–2.0 mm
Abrasive mass flow rate	10 kg/min

Table 6.17 Results of underwater blast cleaning tests (Donker and Richter, 1982)

Parameter	Value
Cleaning rate	$2–7\,\mathrm{m^2/h}$
Maximum roughness	40 µm
Preparation grade	Sa $2^1/_2$ and P Sa $2^1/_2$

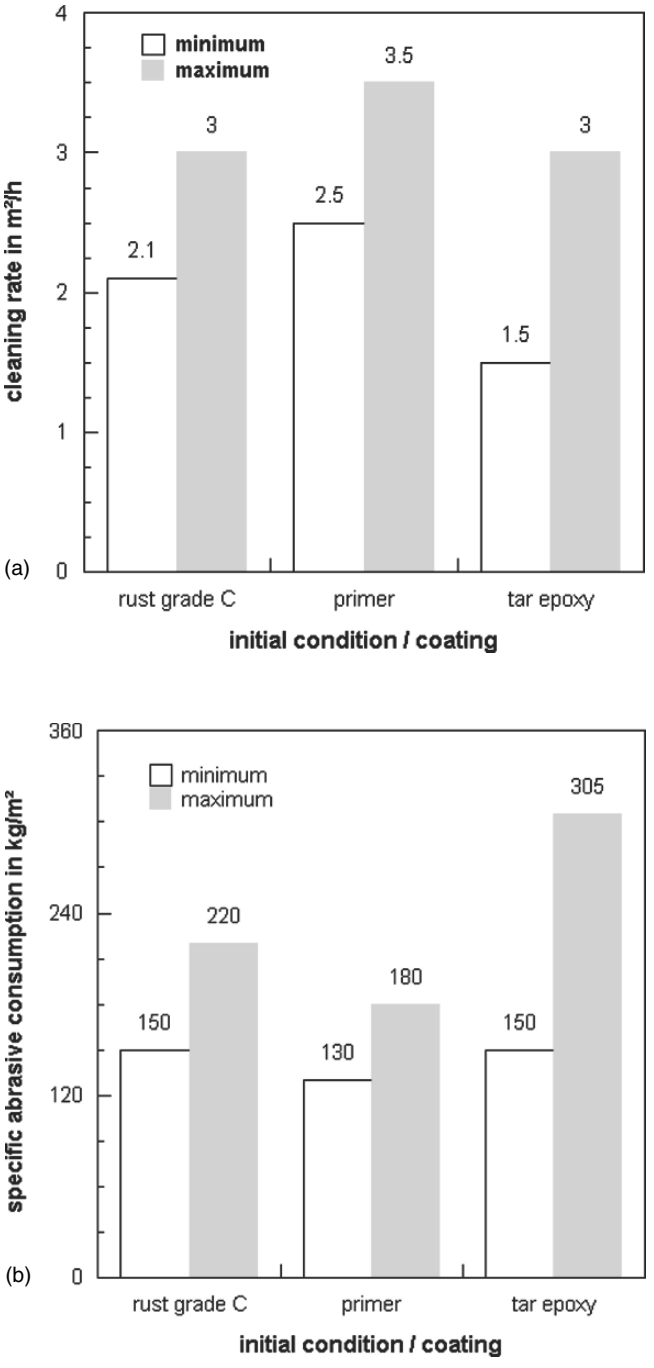

Fig. 6.35 Results of submerged blast cleaning tests (Donker and Richter, 1982); see Table 6.12 for the corresponding operation parameters. (**a**) Cleaning rate; (**b**) Specific abrasive consumption

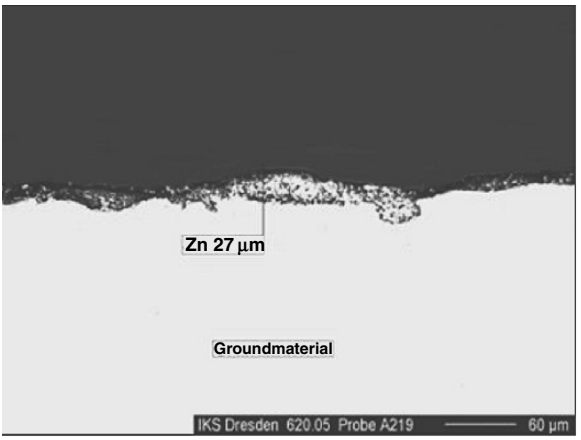

Fig. 6.36 Steel surface blasted with zinc-coated abrasives (Photograph: IKS Dresden)

6.9 Cost Aspects

Dry blast cleaning consumes a notable part of steel refurbishment budgets. A typical value for a 28,400 m^2 project is 42% (Trotter, 2001). For comparison: paint supply cost = 22.1%; painting cost = 20.7% and scaffolding cost = 15.1%. Some cost features for a typical dry blast cleaning system are listed in Table 6.18.

Cost structures for blast cleaning processes are provided in Fig. 6.37. A general cost structure may include the following positions:

- investment air compressor;
- investment blast pot;
- investment hose lines;
- nozzle wear (see Sect. 4.6.2);
- fuel (or electricity, respectively);
- abrasive material (see Chap. 2);
- operators' wages.

The costs of blast cleaning per square metre (m^2) can be calculated as follows:

$$C_{SP} = \frac{(60 \cdot \dot{m}_P \cdot C_P + C_E + C_{LB}) + (60 \cdot \dot{m}_P \cdot C_D + C_{EC} + C_{LC})}{\dot{A}} \qquad (6.37)$$

This is a slightly modified version of an equation suggested by Holt and Austin, (2001). Here, the costs types C_E, C_{LB}, C_{EC} and C_{LC} are given in \$/h, whereas the costs types C_P and C_D are given in \$/kg. The abrasive mass flow rate must be given in kg/min. For given costs for labour, disposal, equipment and abrasive material, it is the abrasive mass flow rate makes the difference.

Table 6.18 Cost structures of various preparation methods (Anonymous, 2002)

Direct operating costs[a]	Preparation method	
	Blast cleaning (Sa 2)[b]	Robotic hydroblasting (HB 2)[c]
Labour		
Crew required	20	6
Labour cost per man/hour	20	40
labour cost/hour	400	240
Total in m^2/h	200	200
Hours spent per 10,000 m^2	50	50
Total labour cost	20,000	12,000
Consumables		
Grit cost and disposal coat/h	1,050	32
Fuel cost/h (machine)	117.5	48.80
Fuel cost/h (vacuum)	–	20
Fuel cost/h (filtration)	–	10
Jets cost/h	–	20
Wear cost (seals, nozzles, etc.)	–	10
Misc. filtration expenses cost/h	–	10
Hours spent per 10,000 m^2	50	50
Total consumables cost	58,360	7,444
Equipment use/maintenance		
Diesel engine cost/h	25	10
Smaller engine cost/h	–	7.50
Compressor cost/h	187.50	–
Hours spent per 10,000 m^2	50	50
Total engine maintenance cost	10,625	875
Total cost to clean 10,000 m^2	88,985	20,319
Cost per square metre	8.90	2.03

[a]All cost in US$; grit consumption: 50 kg/m^2
[b]ISO 8501-1
[c]Hydroblasting Standard, International Paint

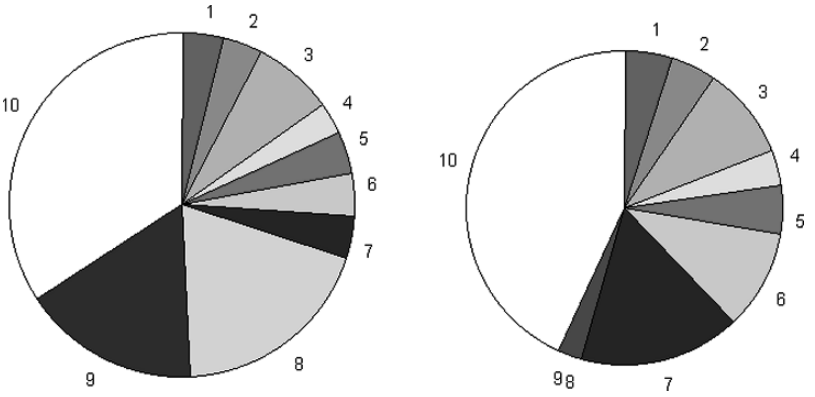

Fig. 6.37 Cost structure of a blast cleaning job (Lyras, 1991). Left: Conventional blast cleaning (1- primer, 2- small equipment, 3- vac truck, 4- compressors, 5- fuel, 6- equipment, 7- abrasive material, 8- disposal, 9- overhead, 10- total labor); Right: recycable blast cleaning (1- primer, 2- small equipment, 3- vac truck, 4- compressors, 5- fuel, 6- equipment, 7- overhead, 8- abrasive material, 9- disposal, 10- total labor)

Table 6.19 Results of comparative cost calculations (Pi and Hoogstrate, 2007)

Parameter	Value	
	Traditional regime	"Optimal" regime
Initial nozzle diameter in mm	3.2	4.4
Nozzle lifetime in hours	300	78
Average cleaning rate in m^2/h	3.8	4.2
Number of used nozzles	1	3.46 (4)
Total working time in hours	300	270
Cost in $/m^2$	42.2	38.8
Total cost in	48,411	44,482

Pi and Hoogstrate (2007) developed an alternative cost calculation model which in particular considered effects of nozzle wear. These authors introduced the concept of an "*optimal exchange nozzle diameter*". This parameter corresponds to the optimum lifetime of a blast cleaning nozzle. Results of calculations are provided in Table 6.19.

Chapter 7
Health, Safety and Environment

7.1 Safety Features of Blast Cleaning

7.1.1 General Safety Aspects

General aspects of health, safety and environment (HSE) for blast cleaning applications are summarised in Fig. 7.1. ISO 12944-4 states the following for surface preparation in general: "*All relevant health and safety regulation shall be observed.*" Blast cleaning owns an injury potential. General sources of danger to blast cleaning operators include the following:

- reactive forces generated by the exiting air-abrasive mixture (see Sect. 6.6.4);
- hose movements;
- uncontrolled escape of pressurised air;
- damaged parts being under pressure;
- dust and aerosol formation;
- sound emitted from equipment and blasting jet;
- impact from rebounding abrasive material and debris from the impact point.

It is generally recommended to carry out a risk assessment of the actual environment where a blast cleaning job will be done before starting the job. This risk assessment may include (French, 1998):

- how access is to be gained?
- is there a need for scaffolding?
- is there confined space?
- what is the surface like where the operators will have to stand?
- the availability of day light or artificial light;
- the presence of electrical supplies/equipment;
- nature of contaminate: Is it toxic? Is it a pathogen? Is it asbestos based? Is it harmful or corrosive?
- general layout that will allow visual contact between the blast cleaning team;
- permit requirements;